



Contents lists available at ScienceDirect

Science of the Total Environment

journal homepage: www.elsevier.com/locate/scitotenv

Deglaciation and its impact on permafrost and rock glacier evolution: New insight from two adjacent cirques in Austria☆

Andreas Kellerer-Pirklbauer^{a,*}, Viktor Kaufmann^b

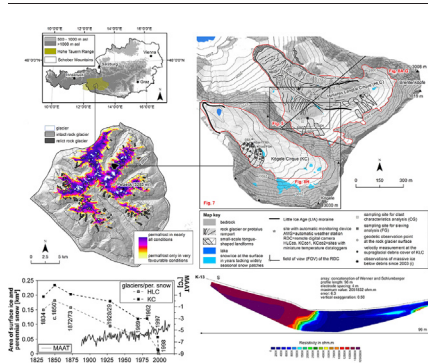
^a Department of Geography and Regional Science, Working Group Alpine Landscape Dynamics (ALADYN), University of Graz, Heinrichstrasse 36, 8010 Graz, Austria

^b Institute of Geodesy, Remote Sensing and Photogrammetry Working Group, Graz University of Technology, Steyrergasse 30, 8010 Graz, Austria

HIGHLIGHTS

- Glacial-to-periglacial landscape change analysed for a 182-year period
- Buried sedimentary ice in a rock glacier detected by different methods
- Low mass losses in 1954–2002 and much higher mass losses since then
- Terrain analysis and geoelectrics indicate a complex rock glacier structure.
- No clear warming or cooling trend in ground temperature in 2006–2016

GRAPHICAL ABSTRACT



ARTICLE INFO

Article history:

Received 31 December 2016

Received in revised form 9 October 2017

Accepted 10 October 2017

Available online xxxx

Keywords:

Alpine deglaciation

Paraglacial processes

Rock glacier evolution

Rock glacier mass balance

Supraglacial debris cover

Debris cover thermal regime

ABSTRACT

Glaciers and permafrost are strongly linked to each other in mid-latitude mountain regions particularly with polythermal glaciers. This linkage is not only climatically defined but also in terms of geomorphic and glaciological processes. We studied two adjacent cirques located in the Central Austria. We focussed on the deglaciation since the Little Ice Age (LIA) maximum (c.1850 CE) and its relevance for permafrost and rock glacier evolution since then. One cirque is occupied by a glacier remnant whereas the second one is occupied by an active rock glacier which was partly overridden by a glacier during the LIA. We applied a multidisciplinary approach using field-based techniques including geoelectrics, geodetic measurements, and automatic monitoring as well as historic maps and photographs, remote sensing, and digital terrain analysis. Results indicate almost complete deglaciation by the end of the last millennium. Small-scale tongue-shaped landforms of complex origin formed during the last decades at finer-grained slope deposits below the cirque headwalls. Field evidences and geophysics results proved the existence of widespread sedimentary ice beneath a thin veneer of debris at these slopes. The variable thickness of the debris layer has a major impact on differential ablation and landform evolution in both cirques. The comparison of digital elevation models revealed clear mass losses at both cirques with low rates between 1954 and 2002 and significantly higher rates since then. The central and lower part of the rock glacier moves fast transporting sediments and ice downvalley. In contrast, the upper part of the rock glacier is characterised by low debris and ice input rates. Both effects cause a significant decoupling of the main rock glacier body from its nourishment area leading eventually to rock glacier starvation. This study demonstrates the importance of a decadal-scale and multidisciplinary research approach in determining the development of alpine landforms over both space and time.

© 2017 Elsevier B.V. All rights reserved.

☆ Special Issue: The environmental consequences of permafrost degradation in a changing climate.

* Corresponding author.

E-mail addresses: andreas.kellerer@uni-graz.at (A. Kellerer-Pirklbauer), viktor.kaufmann@tugraz.at (V. Kaufmann).

1. Introduction

A warming climate might cause substantial changes in the cryosphere leading to morphological responses. The withdrawal of glacier ice, for instance, commonly exposes a landscape that is susceptible to rapid morphological changes causing erosion and sedimentation at rates greatly exceeding background denudation rates (Ryder, 1971; Ballantyne, 2002). Deglaciated slopes overlooking a receding glacier might contribute substantially to the formation and further evolution of a supraglacial debris cover below (Kellerer-Pirklbauer, 2008). Deglaciation can also lead to permafrost formation in locations with favourable topoclimatic conditions (Wegmann et al., 1998; Kneisel, 2003). Changes in the thermal regime in rock walls above a glacier might further increase debris input on the remaining ice below if, for instance, freeze-thaw cycles increase in their frequency, magnitude or duration (Matsuoka and Murton, 2008).

The initial formation or the enlargement of a debris layer in thickness and spatial extent will protect the underlying ice if a critical debris thickness is exceeded causing a reduction in the rate of ablation by shielding the ice from atmospheric heat and insolation (Østrem, 1959; Mattson et al., 1993). This might influence the dynamical and melting behaviour of a glacier (e.g. Deline, 2005; Kellerer-Pirklbauer et al., 2008; Juen et al., 2014). Different types of numerical models have been developed in the past to quantify this sub-debris layer melt rates (Nicholson and Benn, 2006; Reid and Brock, 2010; Juen et al., 2014).

Degrading ice can survive for a long period of time under a protecting debris cover (Whalley and Martin, 1992; Krüger and Kjær, 2000; Everest and Bradwell, 2003). Such glacier or sedimentary ice might get incorporated into a permafrost body such as a rock glacier particularly if the thickness of the subglacial debris cover exceeds the thickness of the active layer (cf. Berthling, 2011; Monnier and Kinnard, 2015). Such buried lenses of massive ice in rock glaciers might get detected by geophysical measurements (Evin & Fabre, 1990; Lugon et al., 2004; Ribolini et al., 2007, 2010). Active rock glaciers are creep phenomena of permafrost in high-relief terrain moving slowly downvalley or downslope often characterised by distinct flow structures with ridges and furrows (Barsch, 1996; Haeberli et al., 2006). Berthling (2011) proposed a genetic definition where active rock glaciers are visible expressions of cumulative deformation by long-term creep of ice/debris mixtures under permafrost conditions.

Active rock glaciers consist mainly of two components: ice (congelation and/or sedimentary/'glacier' ice) and lithological material (periglacially and/or glacially derived rock fragments of different grain size). Liquid water is a further – at least seasonal – component. The formation period of rock glaciers lasts centuries to millennia as judged from relative (Kellerer-Pirklbauer et al., 2008) or absolute (Kraimer et al., 2015) dating approaches. Climate variability in such long time scales as for instance the Holocene is high (e.g. Mayewski et al., 2004) and rock glaciers experience therefore strong variations in the rate of nourishment and the ratio between ice and debris input onto the rock glacier system over time.

Studies on the relationship between rock glaciers and climate revealed that the mean annual air temperature at the rooting zone of active rock glaciers is usually only slightly higher (if at all) than at nearby equilibrium line altitudes (ELA) of glaciers. Or the annual precipitation at the rooting zone of rock glaciers is only slightly lower compared to nearby ELAs of glaciers (Haeberli, 1983; Brazier et al., 1998; Humlum, 1998). This indicates the high sensitivity of rock glacier formation and evolution to cooler and/or more humid conditions and their close climatic relationship to glaciers. Complete understanding regarding rock glacier evolution such as incipient formation, entire development period, variations in nourishment rate and the ratio changes between ice and rock input over a long time span is not sufficiently known and not easy to decipher. However, a close spatial and genetic relationship between glaciers and rock glaciers has been frequently described (Etzelmüller and Hagen, 2005; Monnier and Kinnard, 2015; Janke et al., 2015).

In this study we investigated two adjacent cirques located in the Central Alps of Austria. The two cirques are the Hinteres Langtal Cirque (HLC) and the Kögele Cirque (KC). Climatic, geological, and topographical conditions in both cirques are comparable. Kellerer-Pirklbauer and Kaufmann (2007) presented from these two cirques first data on glaciation and snow changes since the 19th century, the formation of small-scale tongue-shaped landforms in the talus slopes below the cirque headwalls and discussed their age, and possible relationship to permafrost. Here we are going further into detail using additional data based on field work, automatic climate and ground climate monitoring, remote sensing, and digital terrain analysis in order to assess the landscape dynamics in high-alpine cirques after superficial deglaciation located in a permafrost friendly environment. We focussed on (a) glaciation and nival changes between the 1830's and today and recent perennial snow cover survival, (b) geomorphological evolution since 1954 and present geomorphological conditions, and (c) possible permafrost conditions and changes in the decade 2006–2016. The aim of this study is therefore to increase the understanding of the relationship between deglaciation, paraglacial landscape response, and rock glacier evolution and dynamics in a changing environment of a mid-latitude mountain region.

2. Study area

The two studied cirques are located in the central part of the Schober Mountains, a subunit of the Hohe Tauern Range (Fig. 1A). The Hohe Tauern Range covers some 6000 km² and is located primarily in Austria and to a minor extent in Italy. The subunit Schober Mountains extends for 390 km², consists of different types of crystalline rocks, and reaches with Mt. Petzeck its highest elevation (3283 m asl). The mean annual air temperature at 2500 m asl in the Central Schober Mountains increased from –2.08 °C in 1961–1983 to –1.35 °C in 1984–2006 (Taucher et al., 2009; Taucher, 2010). According to the same authors mean annual precipitation was about 2000 mm in 2500 m asl during the period 1961–2006 without a statistical significant trend.

Glaciation is limited to a few positions at the foot of rock faces in northern expositions and at high elevations (Fig. 1B). The mean size of all glaciers in the Schober Mountains does not exceed 0.14 km² ($n = 26$, total area 3.5 km²) (Fischer et al., 2015). Furthermore, most of the glaciers are partly covered by a supraglacial debris cover (Lieb, 1987) influencing glacier ablation (Kellerer-Pirklbauer et al., 2005). Permafrost modelling indicates widespread existence of permafrost (Boeckli et al., 2012). Permafrost is relevant for the 86 active and inactive rock glaciers (Kellerer-Pirklbauer et al., 2012) in the Schober Mountains (Fig. 1B).

The study area consists of the two adjacent cirques HLC and KC which cover a total area of 1.1 km² (Figs. 1C, 2). The former cirque is occupied by an active rock glacier, the latter cirque by a debris-covered glacier remnant. Both cirques are orientated towards northwest with high crests and mountain tops exceeding 3000 m asl. The lower part of the KC is characterised by a distinct latero-terminal moraine ridge which was formed during the Little Ice Age (LIA) with its last glaciation maximum around 1850 CE. On the proximal side of this complex moraine ridge a small outwash or sandur plain (Fig. 2F) with a shallow lake was formed since then. The altitude range of the entire cirque is 2620–3030 m asl (Fig. 1C).

HLC is covered by the tongue-shaped Hinteres Langtalkar Rock Glacier. The rock glacier is 900 m long, up to 300 m wide, covers an area of 0.17 km², consists of mica-schist and amphibolites and ranges from 2455 to 2720 m asl (Avian et al., 2005). Its dimensions make this rock glacier one of the larger rock glaciers of the Central Alps (Kellerer-Pirklbauer et al., 2012). The rock glacier surface is characterised by well-developed longitudinal and transversal ridges and furrows on the surface (Fig. 2A). The talus slopes behind are to some extent separated from the rock glacier body by two rooting zone depressions (Fig. 2B, C).

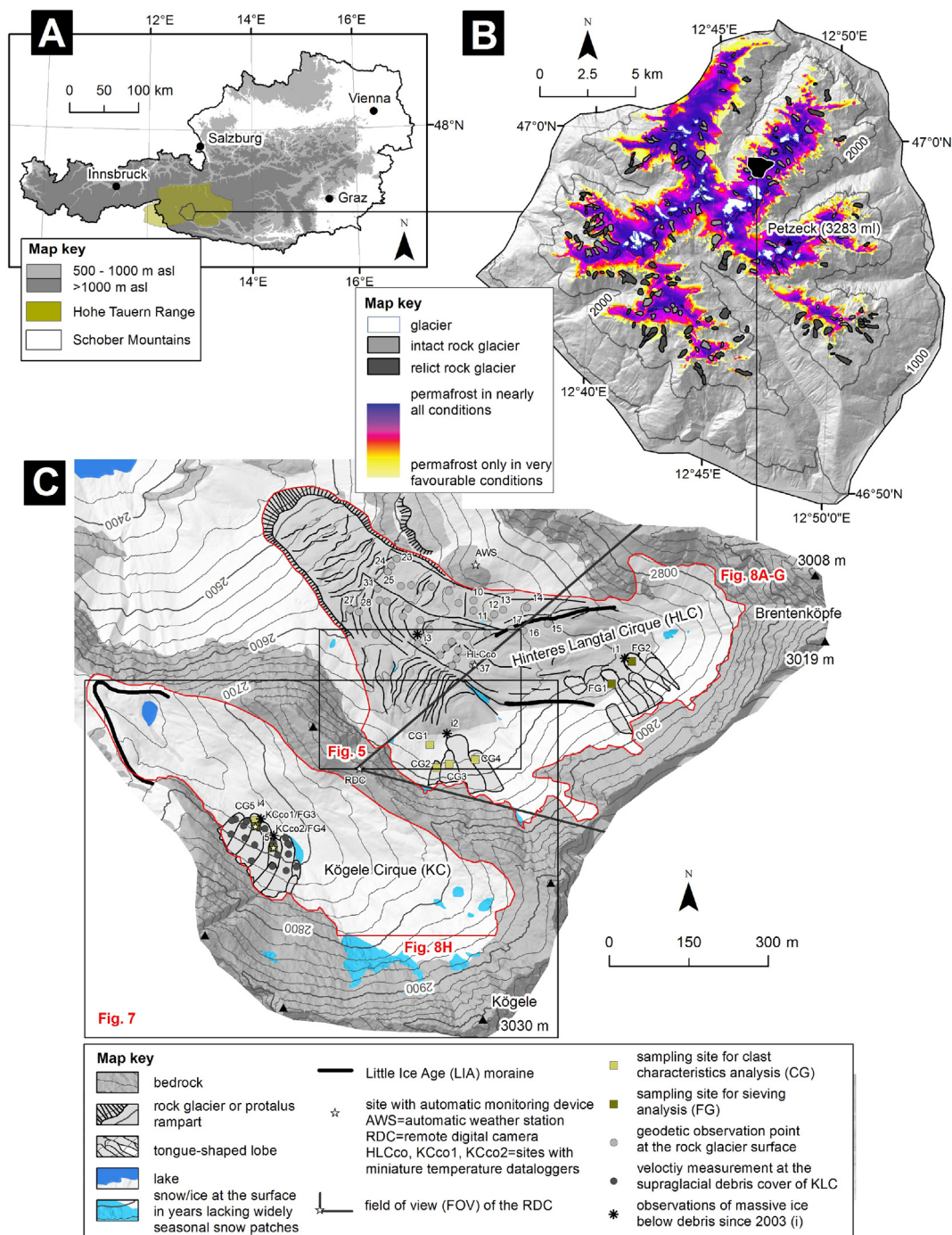


Fig. 1. Study area: (A) Location of the Hohe Tauern Range, the Schober Mountains and the study area in Austria. (B) Relative position of the study area within the Schober Mountains depicting the spatial distribution of glaciers (Fischer et al., 2015), rock glaciers (Kellerer-Pirklbauer et al., 2012), and modelled permafrost (Boeckli et al., 2012). (C) Detailed map of the study area with Kögele Cirque (KC) in the south and Hinteres Langtal Cirque (HLC) in the north. Measurement, monitoring, and sampling sites as well as massive ice sightings since 2003 are indicated.

The front of the rock glacier advanced by 80 m (horizontal component) between 1991 and 1998 (Kaufmann and Ladstädter, 2003, 2010). First distinct changes at the rock glacier surface were detected in the aerial photographs of 1997 with the formation of cracks at the surface and destabilisation of the front (Avian et al., 2005). Since about two decades the frontal part and the entire lower part of the rock glacier tongue is strongly influenced by disintegration through enhanced strain causing active sliding (e.g. Avian et al., 2005, 2008, 2009). Annual rock glacier movement variation is in accordance to other monitored rock glaciers in the region (Delaloye et al., 2008) due to the strong relationship between

rock glacier velocity variability and climate (Kellerer-Pirklbauer and Kaufmann, 2012).

3. Material and methods

3.1. Superficial delineation of ice and snow

Reconstruction of the superficial deglaciation since the LIA and of the retreat of perennial snow cover for the recent past was accomplished for the years 1834, c.1850 (LIA-maximum), 1872/73, 1928/29, 1969, 1982,

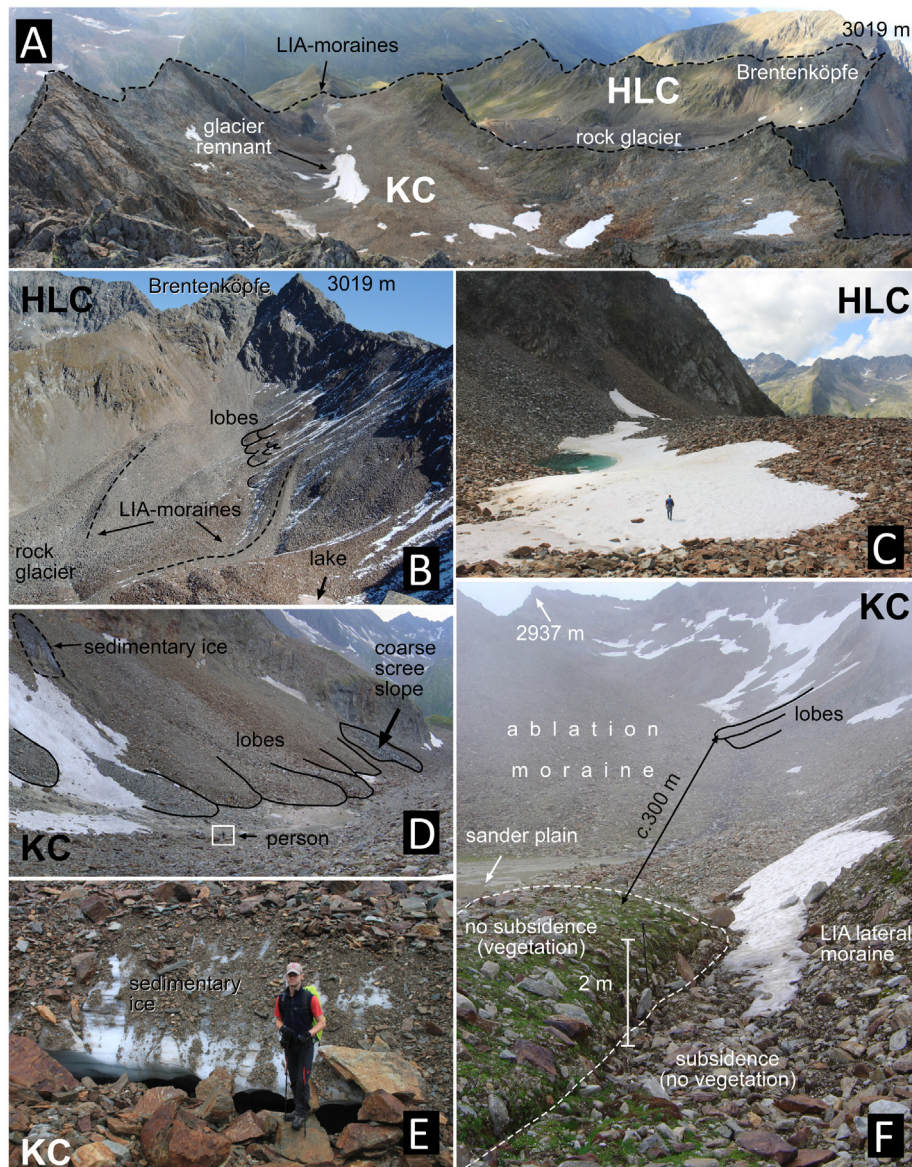


Fig. 2. Terrestrial views of the study area: (A) The catchment areas of both cirques as seen from the summit of Kögele (3030 m); (B) north-eastern part of HLC as seen from the remote digital camera (RDC) site; (C) rooting zone depression at the southern part of HLC with an ephemeral lake (20.08.2010) at the margin of a snow patch below a talus slope (cf. Fig. 5); (D) distinct tongue-shaped landforms atop the glacier remnant in the KC (note the sedimentary ice outcrop and the person in the white box for scale); (E) sedimentary ice outcrop in the KC; note the layered structure and the void; (F) unvegetated flat and unstable depression caused by thaw subsidence at the inner margin of the LIA-lateral moraine in the KC at 2630 m asl. Note the distinct near vertical slope (c.2 m) and its close relationship with the late-lying snow patch. Lobes in the background are schematically retraced for orientation (all photos by the authors).

1997, 1998 using morphological evidences (latero-terminal moraines), historical maps, and terrestrial and aerial photographs (Table 1). Observed massive sedimentary ice outcrops in the HLC were mapped during different field trips since 2003.

3.2. Landform mapping and debris characteristics

Distinct, rather small-scale lobes (in most cases tongue-shaped in plan view) located at the slopes below the cirque headwalls were mapped using orthophotos, digital elevation models (DEM) (Table 1), and field mapping (Fig. 2B, D). These lobes are considered as relevant for rock glacier nourishment in the HLC. It was at the begin of this study not clear if these lobes are incipient rock glaciers, solifluction features, landforms which evolved due to scree sliding over a debris-covered glacier remnant or a mix of thereof. Average width, length and area of the upper surface (tread) and height of frontal slope (riser) were quantified. The length represents the downslope distance

between the headwall or significant nick-point of slope and the lower end of the small-scale tongue-shaped landforms (Matsuoka et al., 2005). The length-to-width ratio (L/W) distinguishes tongue-shaped forms ($L/W > 1$) from lobate forms ($L/W < 1$) (Wahrhaftig and Cox, 1959). A detailed description of these lobes was given by Kellerer-Pirklbauer and Kaufmann (2007).

Clast size and shape was measured at five different sites. In four cases this was done at the surface of the above mentioned lobes (dominated by brownish mica schist) and in one case at a scree slope (dominated by greyish, coarser amphibolite) (Fig. 1C). Clast shape and size was calculated through the measurement of long (a) intermediate (b) and short-axes (c) of 30–100 ‘typical’ clasts per sampling site. Only clasts with an a -axes exceeding 5 cm were considered. The sampling sites were kept as small as possible (maximum diameter of sampling site of 10 m). The b -axis was used as an indicator of clast size. Sorting for each sample was determined by calculating the median and interquartile range (Wilson, 1990). For graphical representation of

Table 1

Historic maps and photographs, aerial photographs and digital elevation models (DEM) used in this study. Abbreviations: BEV = Austrian Federal Office of Metrology and Surveying; BF = Bildflug Fischer, Austria; TIRIS = geographical information service of the federal government of Tyrol; KAGIS = geographical information service of the federal government of Carinthia.

Historic maps and photographs					
Year	Source and scale		Annotation	References	
1834	Franziseische Landes-aufnahme (Zweite Landesaufnahme); 'Kronlandskarte', scale 1:28,800		First cartographic document of glaciers in this area	Kellerer-Pirklbauer and Kaufmann (2007); Photograph of the Schober Mountains as seen from Großglockner mountain, Gustav Jägermayer, summer 1863. (c) Albertina, Vienna, http://www.albertina.at	
c.1850	Field mapping of the Little Ice Age (LIA)-moraines in both cirques		Extent of perennial snow field in the southern part of the HLC was estimated because of missing moraine ridges using the 1834 and 1872/73 stages and a photograph from 1863		
1872/73	Franzisco-Josephinische Landesaufnahme (Dritte Landesaufnahme), 'Sektionsblatt'; sheet 5249/2; scale 1:25,000		Cartographic representation of the two glaciers in the map is rather poor and fuzzy		
1928/29	Österreichische Karte 1:25,000 der fünften, Landesaufnahme; sheet 179/2 Debanttal		First map showing contour lines and glacier boundaries with good quality		
Aerial photographs					
Date	Source	Image scale	Focal length (mm)	Type of film	References
24.09.1954	BEV	1: 15,800	210	Black-and-white	Kellerer-Pirklbauer and Kaufmann (2007); Kaufmann and Ladstädter (2010)
09.10.1969	BEV	1: 29,100	153	Black-and-white	
05.09.1974	BEV	1: 10,000	210	Black-and-white	
04.09.1991	BEV	1: 34,400	153	Black-and-white	
24.09.1997	BEV	1: 32,600	153	Color infrared	
26.08.1998	BF	1: 10,500	152	Black-and-white	
18.09.2002	TIRIS	1: 13,600	305	Color	
21.09.2006	BEV	1: 15,600	304	Color	
08.09.2009	KAGIS	1: 16,600	305	Color	
Digital elevation models (DEM)					
Date/year	Based on:		Grid (m)	Accuracy z (m)	References
24.09.1954	Aerial photographs		1	±0.34	Kaufmann and Ladstädter (2010); Mikl (2016)
05.09.1974	Aerial photographs		2	±0.11	
26.08.1998	Aerial photographs		1/2	±0.11	
18.09.2002	Aerial photographs		1	±0.14	
21.09.2006	Aerial photographs		1	±0.16	
Summer 2012	Airborne laserscanning (ALS)		1	No data provided	Source KAGIS

particle shape, triangular diagrams (Benn and Ballantyne, 1993; Sneed and Folk, 1958) were produced using the triangular diagram plotting spreadsheet (TRI-PLOT; Graham and Midgley, 2000). The form index C40 was calculated. C40 is the percentage of clasts with a form ratio of $c/a \leq 0.4$ (Ballantyne, 1982). A low C40-value is indicative for more blocky shapes.

Sieving analyses of four soil samples collected at two lobes in the HLC and two lobes in the KC, respectively, was carried out to determine the grain size distribution of the fine-grained particles (i.e. sand and smaller). The two sampling sites in the KC are identical with the two sites were ground temperature was monitored as described further below (Fig. 1). In the sieving analysis conventional wet sieving and half to full grade (psi units) intervals in mesh size between sieves were considered.

3.3. Supraglacial debris cover and rock glacier nourishment

The thickness of the supraglacial debris cover in the KC was measured in the field by digging through and measuring the debris layer to solid ice at 34 sites. The thickness data were used to interpolate the

debris cover thickness in the KC applying the inverse distance weighted interpolator in ArcGIS10. An automatic remote digital camera (RDC) system was installed in September 2006 at the ridge between HLC and KC at 2770 m asl (Fig. 1C). This system takes daily images of the north-eastern rooting zone of the rock glacier in the HLC allowing to monitor snow conditions, snow avalanches and mass movement processes in the 0.16 km² large field of view (Kellerer-Pirklbauer and Rieckh, 2016).

3.4. Surface velocity monitoring

Surface velocities of the Hinteres Langtalkar Rock Glacier were compiled for the period 1969–2016 applying digital photogrammetry and geodetic surveys. A geodetic monitoring program was initiated at this rock glacier in 1999. 38 marked geodetic observation points (Fig. 1C) at the rock glacier surface are measured each year in August since then (Kaufmann and Ladstädter, 2010). For reference, eight control points are used in the vicinity of the rock glacier. Representative mean velocity for this rock glacier was retrieved from selected observation points. These points are supposed to belong to areas of similar surficial

movement pattern. Because the upper part of the rock glacier moves substantially slower compared to the lower part two different mean movement values are calculated. The mean value for the upper part is based on nine observation points (# 10–17 and 37), the one of the lower part based on six points (# 23–25, 27, 28 and 31; Fig. 1C).

Photogrammetrically derived horizontal velocity data from identical observation points as the ones for geodetic measurements were used for the period 1969–1991 and 1991–1997. Detailed horizontal displacement vectors for the southern part of the rock glaciers were calculated for the period 1998–2002. The photogrammetric velocity calculations are based on aerial photographs (Table 1) using image matching techniques (ADVM software). Technical details are given in Kaufmann and Ladstädter (2010). Horizontal velocities of the glacier remnant in the KC was measured manually in ArcGIS by analysing 20 distinct boulders at the supraglacial debris cover clearly visible in the orthophotos of 1997, 1998 and 2002. All 20 boulders are located at the surface of lobated-shaped landforms at north-east facing slopes (Fig. 1C). The calculated movement data allowed the comparison of one year (1997–1998) to five years (1998–2002) of horizontal movement. The accuracy of the photogrammetrically-derived velocity data is generally lower compared to the geodetic ones. The accuracy of the former method is in the order of ± 1 to 8 cm/a and primarily depends on the time span of the photographs involved. Numerical values have been calculated for all given time intervals using either stable/non-moving reference areas in the vicinity of the rock glacier and/or by comparison with the geodetically derived velocities if applicable.

3.5. Surface elevation changes

High-resolution multi-temporal DEMs can be efficiently provided either by airborne laser scanning (ALS) or by digital photogrammetry. In this study five digital elevation models based on digital photogrammetry with a grid resolution of 1 or 2 m have been used spanning the period 1954–2006. A detailed description about this procedure is given in Kaufmann and Ladstädter (2010). Finally, the stage 2012 was considered in our analyses using an ALS-derived DEM (Table 1).

The differencing of sequential DEMs to quantify changes in elevation by creating a DEM of difference (DoD) is relevant to geomorphic (Micheletti et al., 2015) and glaciological (Kellerer-Pirklbauer et al., 2008) research questions. At the subarea KC the generation of only one DoD was possible between the two stages 1998 and 2012 related to the limited spatial extents of the other DEMs. At the subarea HLC we were able to consider all six DEMs to create several DoD. The stage 1974 was problematic because of limited aerial photograph quality. For some small and shaded areas in the original aerial photographs particularly at the talus slopes below the steep rock faces data quality was sometimes reduced.

3.6. Ground temperature and climate monitoring

A network for continuous ground surface and near-surface temperature monitoring using miniature temperature dataloggers (MTD) was initiated in September 2006 at several mountain areas in Central and Eastern Austria (Kellerer-Pirklbauer, 2016). In the present study long-term (Sept. 2006 to Aug. 2016) ground temperature data from three sites were used. One site is located at the upper part of the rock glacier in the HLC at 2672 m asl (HLCco). Two dataloggers have been installed at the supraglacial debris cover of the glacier remnant in the KC at 2690 m asl (KCco1) and 2703 m asl (KCco2; Fig. 1C), respectively. The installed MTDs are 3-channel (Model M-Log6) dataloggers equipped with three PT1000 temperature sensors measured hourly the temperature at three different depths below the surface. According to GeoPrecision the PT1000 temperature sensors have an accuracy of ± 0.05 °C, a range -40 to $+100$ °C and a calibration drift <0.01 °C yr⁻¹. Air temperature data have been recorded in the HLC at an

automatic weather station (AWS) located at the top of a rock hummock overlooking the rock glacier (Fig. 1C).

For each ground temperature monitoring site the mean annual ground surface temperature (MAGST), mean annual ground temperature (MAGT) at different depths, thawing degree days (TDD), freezing-degree days (FDD), the surface frost number (F+), and the seasonal snow cover days (SCD) were calculated. For calculating F+ the annual sum of freezing (FDD) and thawing (TDD) degree days per hydrological year are used (Eq. (1)). The result of F+ is dimensionless and indicates: <0.50 = no permafrost; $=0.50$ – 0.60 = sporadic permafrost; 0.60 – 0.67 = discontinuous permafrost; ≥ 0.67 = continuous permafrost (Nelson and Outcalt, 1987).

$$F+ = \frac{\sqrt{|FDD|}}{\sqrt{|FDD|} + \sqrt{TDD}} \quad (1)$$

The SCD was estimated calculating the sum of days with a considerable snow cover damping effect using the 3 cm-values. SCD were counted as such when the weekly standard deviation of the mean daily ground surface temperature was ≤ 0.25 °C (Staub et al., 2016).

Ablation beneath the supraglacial debris cover of KC was estimated taking the ground temperature data from the two sites KCco1 and KCco2, neglecting convective heat fluxes (which surely acts to an unknown extent at both sites), and by using the one-dimensional heat-flux equation for conduction under the assumption of a linear temperature gradient through the debris layer which is thought to be met for timescales ≥ 24 h (Nicholson and Benn, 2006). The conductive heat flux through the debris layer Q_c (W m²) can be calculated as

$$Q_{c+} = -k \frac{(T_i - T_s)}{h_d} \quad (2)$$

where k is the thermal conductivity (W m⁻¹ K⁻¹) of the debris layer, T_i is the ice temperature at the debris–ice contact, T_s is the surface temperature, and h_d is the thickness of the debris layer. The thermal conductivity is the most sensitive parameter and may vary substantially (Nicholson and Benn, 2006). Based on comparison between the DoD-derived mean annual ablation rates (cf. Fig. 8G) and modelling results using different k -values, we considered a rather low value of 0.22 W m⁻¹ K⁻¹ (also used by Marangunic, 2010, Monnier and Kinnard, 2015) as appropriate. The ablation rate M (cm d⁻¹) beneath the debris layer was calculated using the following equation (Nicholson and Benn, 2006; Reid and Brock, 2010)

$$M = \frac{Q_c}{\rho_i L_f} \times 8.64 \cdot 10^6 \quad (3)$$

where ρ_i is the density of ice (900 kg m⁻³), and L_f is the latent heat of fusion (334 kJ kg⁻¹).

3.7. Electrical resistivity tomography

Electrical resistivity tomography (ERT) was accomplished at two profiles in the HLC and, respectively, at 13 profiles in the KC (see Fig. 8 for location). The two ERT profiles at HLC were 490 m (H-1; 50 electrodes, 10 m electrode spacing) and 290 m (H-2; 30 electrodes, 10 m electrode spacing) long applying the Wenner array. Results of the two profiles H-1 and H-2 have been described in Kellerer-Pirklbauer et al. (2014). The 13 ERT profiles in the KC were measured in August 2014 and August 2015 using the GeoTom-2D system (Geolog2000, Starnberg, Germany) with multicore cables. Depending upon the local topography, between 20 and 25 electrodes with 2 or 4 m electrode spacing were used. Salt water was sometimes used to improve electrical contacts. The 13 profile measurements were carried out applying both the Wenner and Schlumberger arrays (Kneisel and Hauck, 2008). ERT data

analysis was carried out in the software RES2DINV concatenating both array-results and using the robust inversion modelling (Loke, 2000).

4. Results

4.1. Evolution of surface ice and snow since the 1830's

The area covered by glaciers in both studied cirques in 1834 was 0.34 km² (Fig. 3B). Some 16 years later, this value increased by 15% (0.39 km²) indicating a notable glacier advance during this period. The two cirque glaciers created distinct terminal (KC) or latero-terminal (HLC) moraines during this LIA maximum stage as indicated in Figs. 1C, 2B and 3A. 0.21 km² of the Kc and 0.18 km² of the HLC have been covered during that time by ice and perennial snow. 5% (KC) to 13% (HLC) of it was lost by 1872/73 decreasing further in spatial extent during the subsequent three decades. The stage of 1928/29 can be regarded as the fading period of the 1920-advance (Lieb, 1987) which is hardly geomorphologically visible in both cirques. 2.9 km² of both cirques were covered by perennial snow and ice at this stage. During the 40 years period 1928/29 to 1969 the total glaciation in both cirques decreased by 38.5%. In 1969 a 0.12 km² large glacier in the KC and two patches with perennial snow and ice in the HLC covering together 0.06 km² existed.

The snow and ice extent in 1982 was very similar to the one of 1969 related to cooler, more-glacier favourable conditions in the late 1970s and early 1980s. Since the end of this glacier-favourable period the ice and snow extent in both cirques decreased dramatically. By 1997

surface ice and perennial snow patches covered 0.05 km² of the KC and only 0.01 km² of the HLC. One year later, only in the KC notable patches of surface ice have been mapped in the aerial photographs. Thus, one might summarise that by the end of the 1990's both niche glaciers disappeared – at least superficially. Since then only very small patches of ice and perennial snow have been found in the most radiation-sheltered locations in both cirques.

Observations of massive ice below debris in the HLC since 2003 have been made at three sites (Fig. 1C). The largest massive ice exposure in the HLC was an up to 20 m long and <2 m high massive ice outcrop at the southern rooting zone of the rock glacier (i2 in Fig. 1C). This outcrop has been observed for the first time in 2006. The other two massive ice observations were rather small in spatial extent: i1 small patch below 30 cm of debris; i3 below 20–30 cm of debris at the upper edge of a transversal furrow. In contrast, massive ice below debris has been observed at two places in the KC particularly at the foot of the steep cirque-headwall (i4 and i5 in Fig. 1C). The most striking outcrop was c.2 m high and several meter long located at the foot of a tongue-shaped landform (i4 in Fig. 1C). This outcrop, characterised by a layered structure, was observed for the first time in 2006 and in subsequent snow-poor summers (Fig. 2E).

As judged from the automatic camera system (operating since 2006) taking daily images and the numerous field trips of both authors during the last decade one can conclude that perennial snow was absent in the KC in 2007 and 2012 and, respectively, absent in the HLC in 2006–2008, 2011, and 2012 (Fig. 3C). This reduction of the spatial extent of surface ice and snow is in accordance with the general warming of the

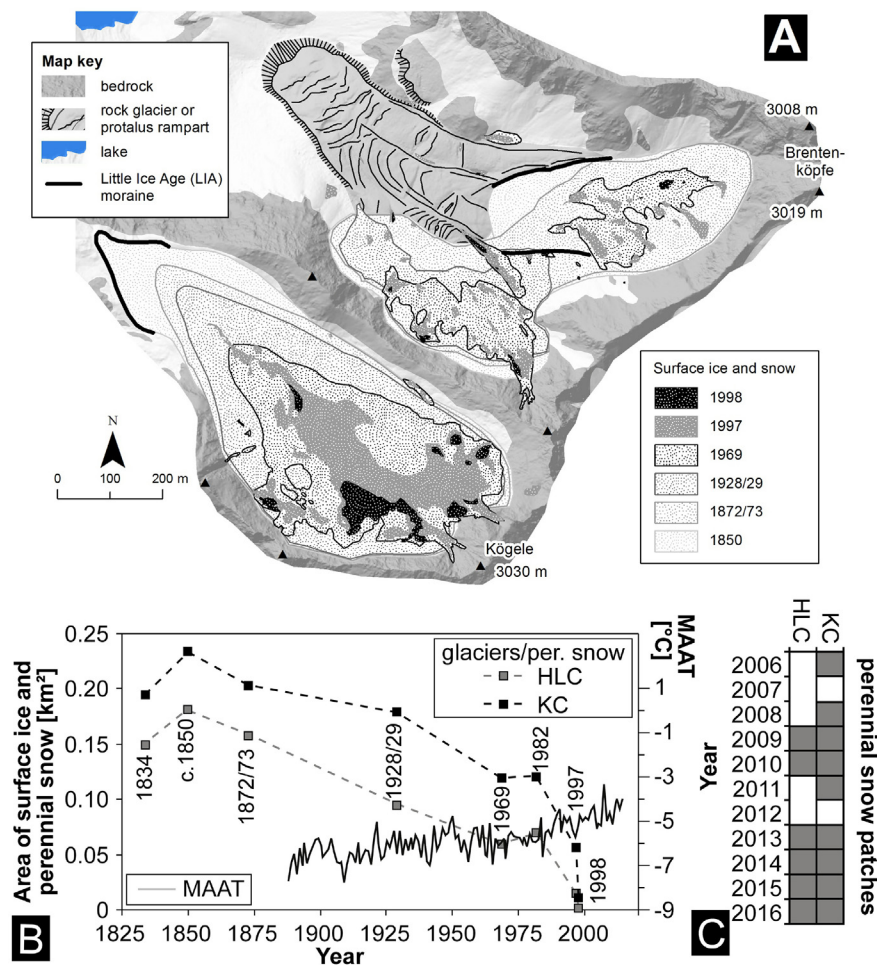


Fig. 3. Change of superficial ice and snow over time: Change in the spatial extent of surface glacier ice and perennial snow patches between 1834 and 1998 depicted in a map (A) and in a diagram (B). (C) Survival of perennial snow patches in the two cirques during the summers 2006–2016. (B) Also depicts the evolution of the mean annual air temperature (glaciological years) at Hoher Sonnbluck since 1887/88 located 15 km NE of the study area at 3106 m asl. For explanation and data source refer to text.

mountains in Austria since the 19th century as revealed by the evolution of the mean annual air temperature at the meteorological observatory Hoher Sonnblick (3106 m asl) located 15 km NE of the study area (Fig. 3B).

4.2. Debris landforms below the cirque headwalls and its movement

Twenty-two small-scale landforms have been mapped below the cirque headwalls in the KC and the HLC (Figs. 1C, 2C, 7). In most cases these landforms are tongue-shaped apart from one of the mapped landform where length equals width. These landforms seem to have been formed from the slope sediments, are not covered by vegetation, and are located in close vicinity of remaining patches of superficial ice and snow particularly in the KC. In the KC nine small-scale tongue-shaped landforms have been mapped all clustering around the SW-margin of the cirque and are exposed to N-NE. At two longitudinal profiles two successive risers appear thus a lower and an upper lobe unit were distinguished. Morphometric analyses reveal: height of the frontal slope 1–3 m, length of the landforms 66–125 m, widths 15–31 m, average slopes 26–30°, and spatial extent of 859–3276 m² covering a total area of 14,424 m². Most of the lobes in the KC have a downvalley-bended appearance at plan view (Figs. 1C, 7) indicating ongoing downward (towards NW) creep of the remaining debris-covered glacier ice.

Horizontal surface velocities of the lobes in the KC have been measured by tracing 20 distinct boulders visible in the orthophotographs of 1997, 1998, and, respectively, 2002 (Fig. 1C). The mean surface velocity of the 20 boulders was 1.02 m in 1997–1998 and 2.85 m in 1997–2002 (i.e. 0.57 m/a). 1-year velocities ranged from 0.45 to 1.60 m. 5-year values ranged from 1.45 to 5.10 m. The 1- and 5-year values of the 20 boulders are significantly ($p < 0.01$) and strongly ($r = 0.73$) correlated indicating a high movement pattern consistency (Fig. 4C).

Small-scale tongue-shaped landforms have also been mapped in the two rooting zones of the Hinteres Langtarkar Rock Glacier (Figs. 1C, 2B). Four different lobes were identified in the SW-rooting zone. All four lobes are orientated towards N and cover 8364 m² in total. Eight lobes were mapped in the northern rooting zone. Here, only at one longitudinal profiles two distinct risers (therefore two separate units) have been distinguished. Morphometric analysis of all HLC lobes reveal: height of the frontal slope 1–6 m, length of the landforms 38–116 m, widths 13–34 m, average slopes 24–34°, and spatial extent 722–3789 m² (sum 17,695 m²). No bending was revealed for the mapped lobes in the HLC.

Detailed image matching analysis showed that the southern part of the rock glacier in the HLC is not entirely moving out of the valley i.e. towards NW as it should be expected considering the general movement direction of the highly active rock glacier. Fig. 5 depicts horizontal displacement vectors derived from aerial photographs from 1998 and 2002 at the southern rooting zone of the rock glacier in the HLC. In total 6849 vectors were computed. The achieved accuracy in vector length is ± 1.3 cm/a. Note in Fig. 5 that the southern-most part of the

rock glacier (the area north of the lake) moved backwards towards the depression which was filled with an ephemeral lake during some years in the recent past. This depression increased during the last decade and was filled in some years at least partly by an ephemeral lake. In the two years 2003 and 2010 a distinct lake has been observed and partly (2010) mapped by GPS. No lake has been observed in 2004, 2006–2009, and 2011–2016. For 2005 we do not know if such a lake existed or not. Fig. 5 shows the extent of the ephemeral lake in 2010 at the southern rooting zone depression mapped by GPS during two field campaigns (cf. Fig. 2c). This lake covered 358 m² on the 20.08.2010. 27 days later the lake level was slightly lower and covered only an area of 155 m² hence reduced its extent by 57%.

4.3. Sediment characteristics and supraglacial debris cover thickness

Sediments were analysed in both cirques focussing on fine material (i.e. sand fraction and smaller; four samples) and the debris (five samples) of the talus slopes below the cirque headwalls. In addition, the thickness of the sediments covering the glacier remnant in the KC – hence the supraglacial debris cover thickness – was measured. The sieving analyses of the four samples (two at each cirque; Fig. 1C) reveal in all cases a dominance of sand with 51.8–72.8% (Fig. 6A). In three out of four cases the silt-and-clay content exceeds 40% suggesting a high relevance of silt and clay as a weathering product of the mica-schist which dominates the bedrock geology of the two cirques.

The largest clasts – in terms of a-, b- and c-axes – have been measured at the scree slope site (CG1) that lacks any sort of a tongue-shaped landform and which is dominated by amphibolites. Mean values at CG1 are 81.5 cm (for a-axis), 52.2 cm (for b), and 30.1 cm (for c), respectively (Fig. 6B). The standard deviation is high for a- (SD = 49.4 cm) and b-axes (SD = 28.8 cm) indicating a wide range of clast sizes on this scree slope. At the four sample sites where small-scale tongue-shaped landforms occur (CG2–CG5) clast sizes are substantially smaller with values of 25.3–45.2 cm for a-axis, 15.5–27.2 cm for b-axis, and 6.2–14.0 cm for c-axis (Fig. 6B). The longest a-axes dimension was measured at the coarse-slope site (CG1) with 210 cm, whereas the longest a-axes at a tongue-shaped landform site was only 107 cm (CG4). In general, the axes dimensions and the SD-values of the four samples taken from the tongue-shaped landforms are comparable to each other.

A more detailed view on the distribution of the b-axes values including median and interquartile range – as a representative indicator of clast size and average size and sorting for each sample – is shown in Fig. 6C. Individual clasts range in size from 3 to 130 cm (3–70 cm without CG1) and mean values from 15.5–52.3 cm (15.5–27.2 cm without HLC1). Sorting is generally better for smaller-sized debris. At the sampling sites CG2, CG4, and CG5 the interquartile range is only 11.25–12.0 cm which indicates well sorted rock material. At site CG3 the mean values for the b-axes (27.2 cm) as well as the interquartile range (20 cm) are the highest of all four sampling sites on small-scale

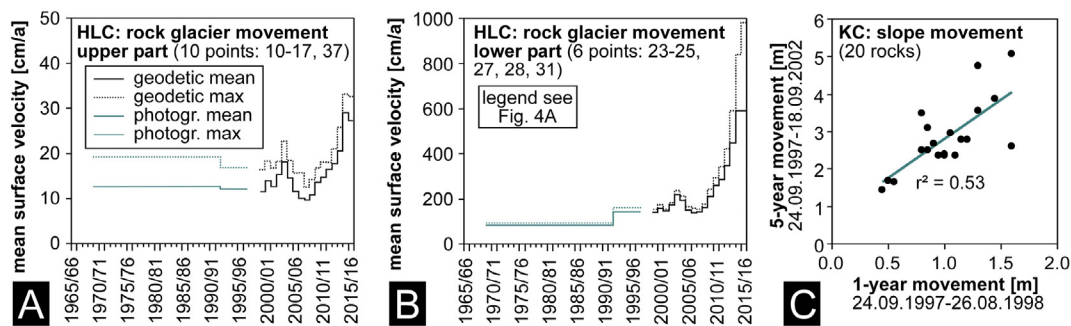


Fig. 4. Mean and maximum values of the annual horizontal surface velocity of the Hinteres Langtarkar Rock Glacier between 1969 and 2016 based on geodetic and photogrammetric measurements and differentiated between the upper/slower part (A) and the lower/faster part (B) (for details see text). (C) Horizontal movement of 20 distinct boulders in the KC during the 1-year period 1997–1998, during the 5-year period 1997–2002, and its relationship. For locations of velocity measurement points see Fig. 1.

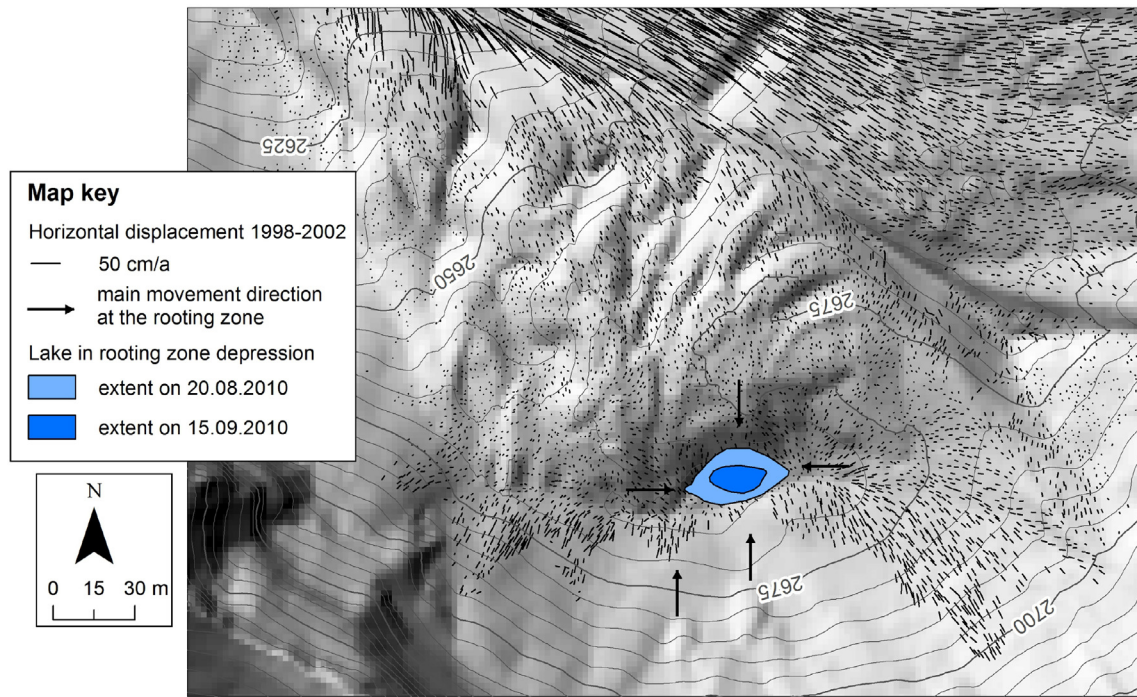


Fig. 5. Horizontal displacement vectors derived from aerial photographs from 1998 and 2002 at the southern rooting zone of the rock glacier in the HLC. Note the peculiar movement pattern around the spoon-shaped depression where in some years an ephemeral lake existed in the past. The extent of an ephemeral lake mapped twice in 2010 by GPS is depicted (cf. Fig. 2c).

tongue-shaped landforms. At the scree slope site CG1, the interquartile range is much higher (27.5 cm) compared to the other four sites indicating poor sorting.

The distribution of the clast shapes at the five sample sites is depicted in Fig. 6D. The ternary graph showing the distribution at the scree slope site (CG1) is completely different to the graphs showing the particle shapes from the other four sites. Most of the clasts of CG1

cluster in the centre of the ternary diagram just below the C40-line. Furthermore, the C40-value at CG1 is the lowest value at all five sites which is indicative for more blocky shapes of the clasts. However, the C40-value at CG1 is only slightly lower as compared to the sampling site CG3 (82) and CG4 (80). The highest percentage of slabs and elongates is found at sites CG2 and CG4 with C40-values of, respectively, 97 and 96.

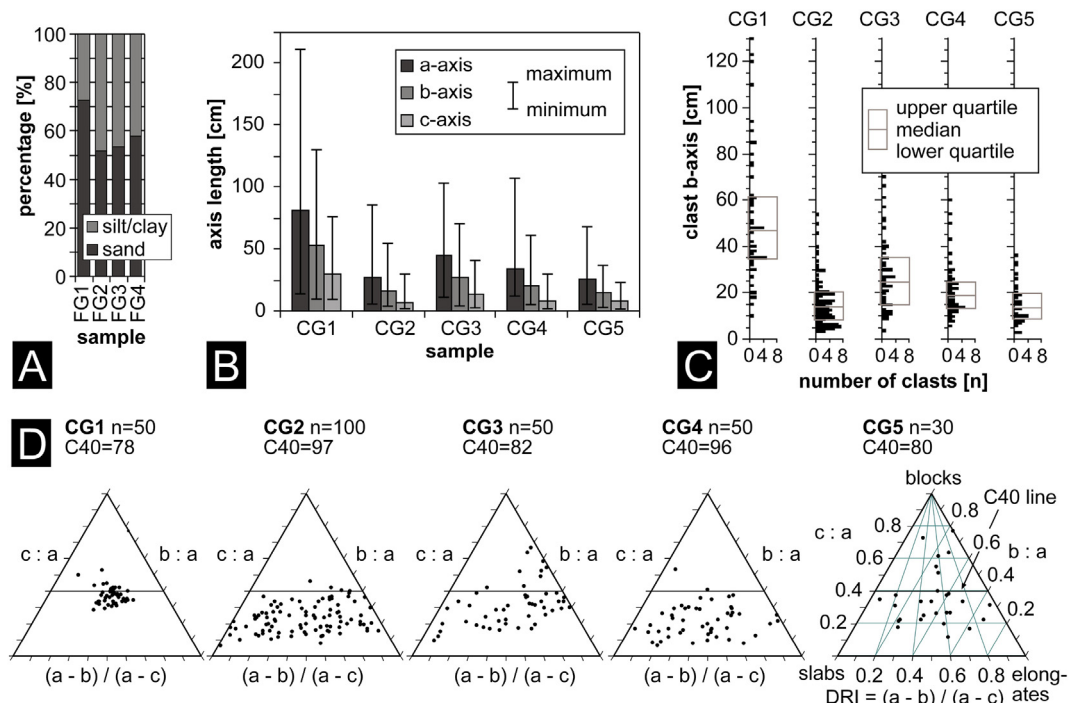


Fig. 6. Sediment characteristics of the talus slopes in the two cirques: (A) sand and silt/clay content of four fine-grained (FG) samples. Mean clast size (B), sorting (C) and shape (D) of five coarse-grained (CG) (≥ 5 cm of the intermediate dimension or b-axis) debris samples. C40 is the percentage of clasts with ratios < 0.4 (C40 line defines the line where $c/a = 0.4$). DRI is the disk-rod index equal to $(a-b)/(a-c)$. For sample locations see Fig. 1.

As judged from the 34 measurement points in the field the supraglacial debris cover in the KC ranges from 0 (at clearly identifiable bedrock outcrops in the cirque) to >70 cm. A general tendency of increasing debris thickness further downvalley has been revealed by these measurements and interpolations (Fig. 7). However, at the NW part of the mapping area digging deeper was difficult. Therefore, it remains unclear by this method how thick the debris mantle is further downvalley and how buried massive sedimentary ice is distributed in the entire KC.

4.4. Rock glacier velocity

Fig. 4A and B depict the mean and maximum annual horizontal surface velocities of the Hinteres Langtalar Rock glacier during a 47-year long period (1969–2016) based on photogrammetric and geodetic data. In this figure the velocity rates are differentiated between the slow-moving upper part (Fig. 4A) and the substantially faster moving lower part (Fig. 4B) (for details see [methods section](#)). Annual mean and maximum values of the upper part were slightly higher in the period 1969–1991 (mean 12.5 cm/a) compared to the period 1991–1997 (mean 12.1 cm/a) suggesting a slight velocity decrease (at least based on the multi-annual photogrammetric data). In contrast, both the mean and maximum horizontal surface velocities of the lower part increased substantially between the periods 1969–1991 (82.4 cm/a) and the period 1991–1997 (142.7 cm/a) indicating speed-up.

The annual horizontal surface velocity data since 1999 give a more detailed picture about interannual changes. Both the annual mean and the maximum surface velocity data show a strong ($r = 0.96$ for mean values; $r = 0.94$ for maximum values) and highly significant ($p < 0.01$) correlation between the lower and upper part of the rock glacier. A first peak in the horizontal surface velocity was reached in the monitoring year 2003/04 at both parts followed by a period of deceleration until 2007/08. Afterwards the rates increased again substantially from year to year with maximum values in 2014/15 (mean upper part: 28.9 cm/a; mean lower part: 600.3 cm/a). The mean values of the last measurement year were slightly lower.

4.5. Volumetric changes of the cirques

Fig. 8 depicts volumetric changes of the two studied cirques during different periods as quantified by several DoDs. Table 2 lists the numeric results regarding the respective relevant areas (cf. Fig. 1C), the mean annual surface elevation changes and the volumetric changes. At HLC the entire sediment transport system of the rock glacier and its talus slope behind has been considered (apart from 1974). Therefore, one might regard this analysis as a geodetically-based rock glacier mass balance analysis with advantages and disadvantages as discussed further below.

Results show for all periods a clear negative mean annual surface elevation change at the HLC with mean values ranging from -0.016 to -0.058 m/a. This implies a change in the mean annual volume of the rock glacier sediment transport system of -4800 to $-15,800$ m³/a. All the DoDs covering the 58-year period 1954 to 2012 reveal a volume loss of the rock glacier sediment transport system of $-435,895$ m³ averaging to -7515 m³/a. The mean surface elevation change of the rock glacier system amounts to -1.59 m which is equivalent to a mean surface lowering of -2.74 cm/a. The only area of substantial surface elevation gain was during all periods the rock glacier front particularly until 1998. After 1998 this general gain-area was influenced by destabilisation of the frontal part hence areas with elevation gain exist next to areas with elevation loss since then. In the rooting zone of the rock glacier in the HLC there was no period of mass gain. Both rooting zones of the rock glacier in the HLC (apart from the norther part of the NE-rooting zone) and the adjacent talus slopes show a general loss of elevation during the 1954–2012 period indicating continuous loss of subsurface ice.

The surface elevation change pattern revealed for the KC is in accordance with the findings in the HLC with the highest values at the foot of the cirque headwalls where massive sedimentary ice is present. However, interestingly the mean annual surface elevation change in the cirque (at least of the area which is covered by the two DEMs 1998 and 2012) is substantially higher to any of the values in the HLC with -0.107 m/a during the 1998–2012 period. This suggests either more widespread sedimentary ice in the KC compared to the HLC rock glacier rooting zones, thicker supraglacial debris in the HLC compared to KC protecting buried ice melt or both.

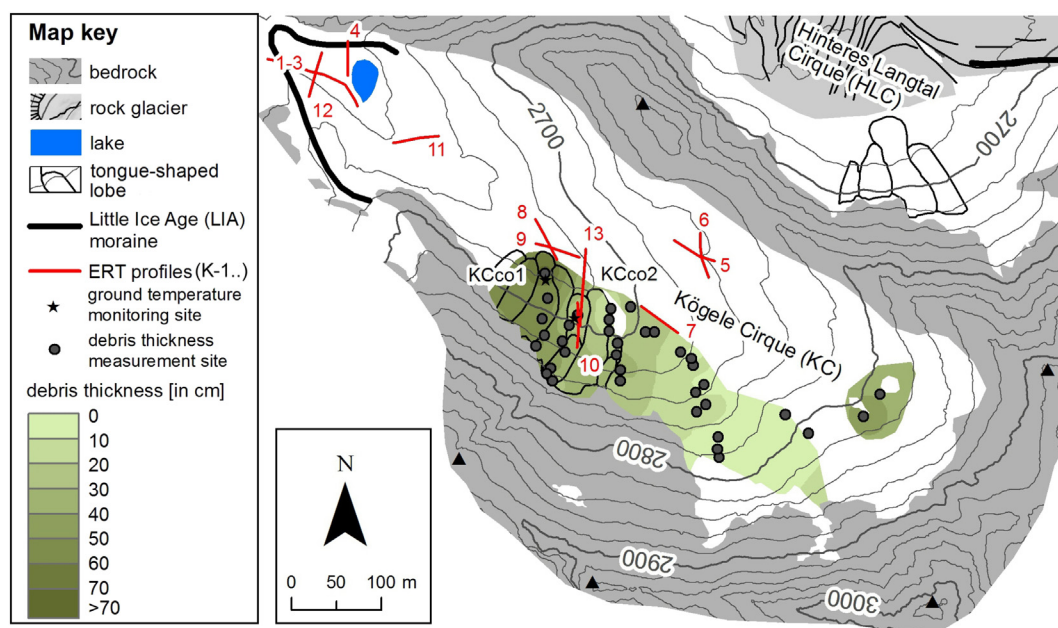


Fig. 7. The supraglacial debris cover in the KC based on 34 field measurements and desktop interpolation. Locations of the small-scale tongue shaped landforms and the 13 ERT profiles are indicated.

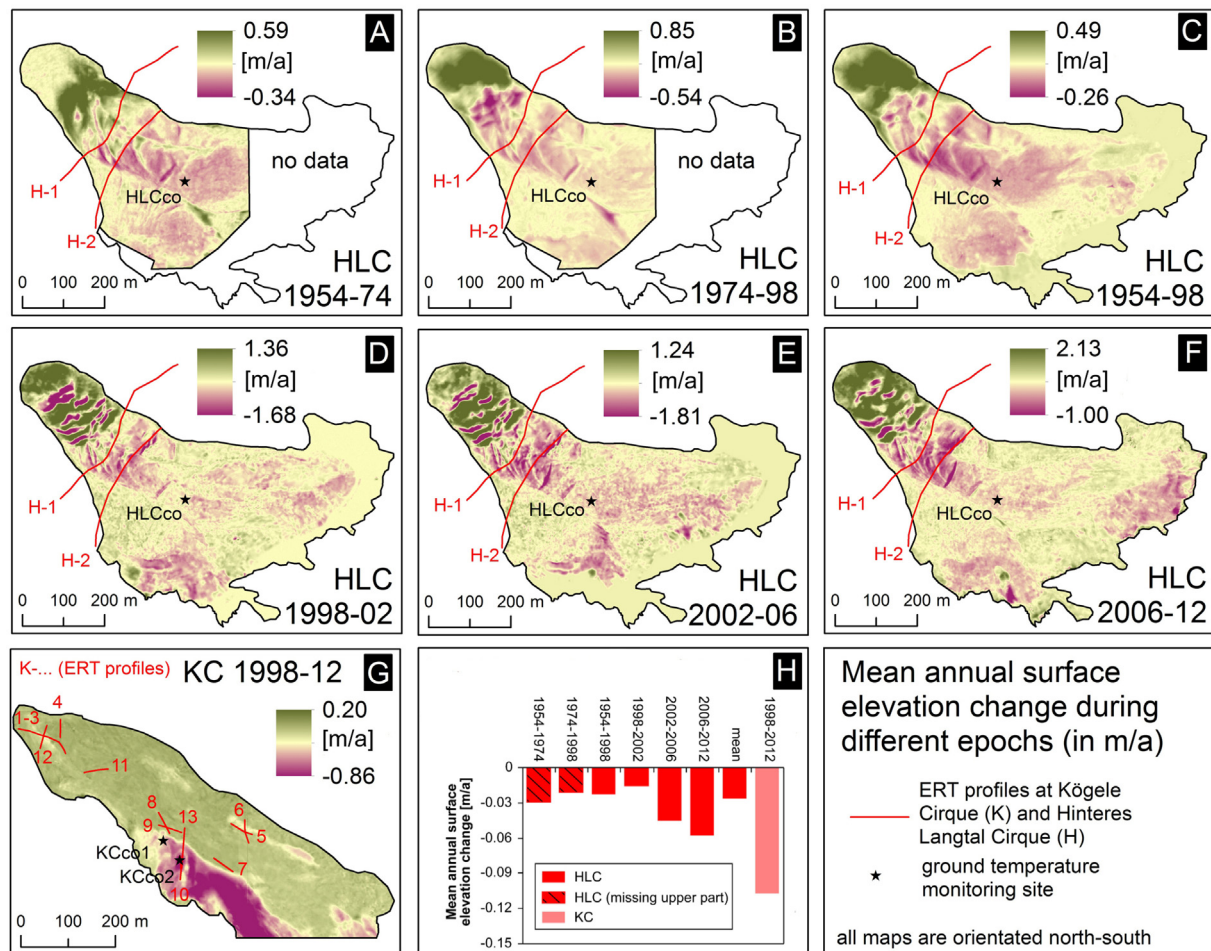


Fig. 8. Mean annual surface elevation change for different epochs at the two cirques HLC (A–F) and KC (G). Graph (H) depicts the mean annual surface elevation change for different periods and for the two different areas as depicted in (A) to (G) as well as the mean for HLC in 1954–2012. Note the different scale values for each map in order to visualise relative differences at its best. Locations of the ERT profiles in HLC (H-1 to H-2) and KLC (1–13) are indicated.

4.6. Ground thermal conditions

Fig. 9 depicts the mean daily ground temperatures, the snow cover days and the subsurface isotherms at three ground temperature monitoring sites HLCco, KCco1, and KCco2 and at the automatic weather station in the HLC during the period 2006–2016. Table 3 lists the analytical results regarding mean annual ground temperature at the surface (MAGST) and at different depths (MAGT), the surface frost number (F+); the thawing degree days at different depths and the snow cover days (SCD) per hydrological year between 2006/07 and 2014/15. At site HLCco, located at 2672 m asl, the mean daily summer temperatures at the surface hardly reaches +15 °C (maximum +16.3 °C) whereas winter temperatures are normally influenced by a prolonged

seasonal snow cover which protects the ground from the very low air temperatures with mean daily temperatures of about –20 °C. Mean ground surface temperatures below the protecting snow cover have been around –5.0 °C indicating permafrost conditions. At site KCco1, located at 2690 m asl, the variation of the mean daily temperatures at the surface and at different depths clearly shows that the seasonal snow is of less importance at this site allowing deep freezing and cool ground temperatures in five out of the ten years with monitoring data.

Whereas mean daily summer temperatures at the surface (maximum 16.1 °C) are comparable to the ones at site HLCco, mean daily winter temperatures frequently reach less than –10 °C. However, in snow richer winters a stable value of around –5 °C is also reached at this site suggesting again permafrost conditions. The minor influence of snow at

Table 2

Surface elevation and volumetric changes based on DEMs of difference (DoD) in the two study areas for different periods. For spatial extent of the relevant areas see Fig. 8.

Site	Period	Considered area (m ²)	Mean annual surface elevation change (m/a)				Mean annual change (m ³ /a)	Total volume change (m ³)
			Min	Max	Mean	SD		
HLC	1954–1974 ^a	162,376	–0.345	0.584	–0.029	±0.122	–4789.4	–95,789
	1974 ^a –1998	162,376	–0.542	0.845	–0.021	±0.167	–3464.9	–83,158
	1954–1998	273,913	–0.264	0.486	–0.023	±0.089	–6229.5	–274,100
	1998–2002	273,913	–1.679	1.359	–0.016	±0.225	–4399.7	–17,599
	2002–2006	273,913	–1.805	1.229	–0.045	±0.198	–12,348.7	–49,395
HLC	2006–2012	273,913	–1.001	2.133	–0.058	±0.183	–15,800.4	–94,802
	KC	1998–2012	167,136	–0.860	0.199	–0.107	±0.175	–17,851.8

^a The spatial extent of the 1974-DEM was not covering the entire rock glacier mass transport system.

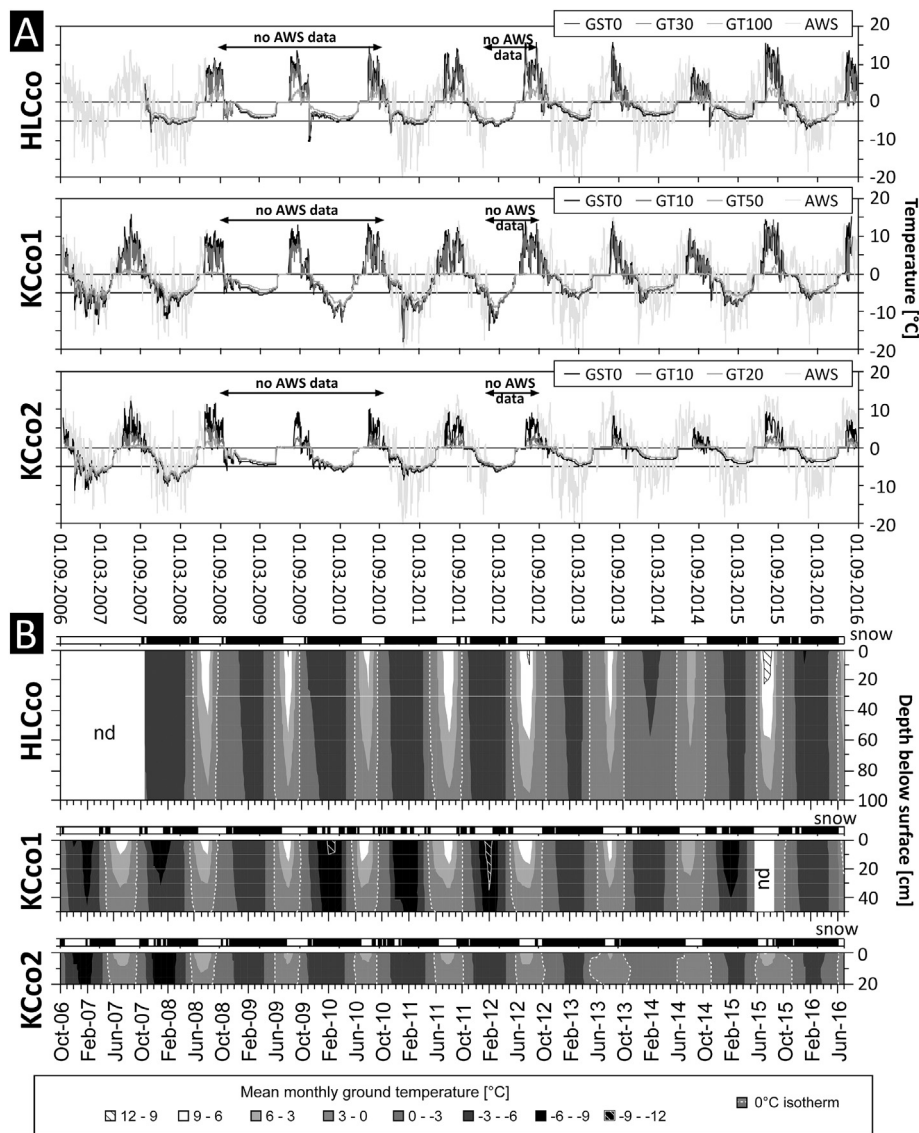


Fig. 9. Ground thermal and climatic conditions in the two cirques between September 2006 and August 2016. (A) mean daily ground temperature (at the surface and at three different depths) at the three ground temperature monitoring sites and the air temperature at the AWS. (B) snow cover (black) and snow free (white) days as well as the subsurface isotherms (3 °C intervals) based on mean monthly values at the three monitoring sites. The dashed line marks the 0 °C isotherm. nd = no data. For locations of sites see Fig. 1.

this site also implies that the MAGST at KCCo1 was 0.25 °C to 0.75 °C cooler during the monitoring period compared to HLCco. Finally, at site KCCo2, located at 2703 m asl, the variation of the mean daily temperatures at the surface and at different depths shows again a strong influence of a damping winter snow cover. Furthermore, this site is the coolest of the three sites with mean daily summer temperatures barely reaching the 10 °C level (maximum MAGST 12.4 °C). In contrast, the lowest daily mean temperature measured during the entire monitoring period at the ground surface was only – 11.2 °C yielding a temperature amplitude – based on daily mean values – of only 23.6 °C during the 2006–2016 monitoring period. In contrast, this temperature amplitude was 27.0 °C at HLCco and 33.8 °C at KCCo1.

The sites HLCco and KCCo2 are both strongly influenced by a seasonal snow cover with on average >210 SCD per year. As illustrated in Fig. 9B, the length of the SCD is substantially shorter and more interrupted at the third site KCCo1 (mean SCD 120 days) related to the more wind-exposed position of this monitoring site. Fig. 9B depicts furthermore that the coolest winter temperatures have been observed during snow-poor winters at site KCCo1 with mean monthly values below – 9 °C at the surface and down to 30 cm into the debris layer. The length of the SCD correlates negatively with the TDD indicating that the more

SCD during a year, the less warming occurs at the surface and at the sub-surface. Regarding summer temperatures at the surface and within the debris layer it is shown that warming – and also cooling – at site HLCco reacts fast attributed to convective heat transport through the open voids (fast cooling and warming, respectively, of the entire 1 m profile). Mean monthly summer temperatures at this site exceed the 9 °C-level during warm summers. In contrast, warming and cooling of the debris layers at sites KCCo1 and KCCo2 is also influenced by heat conduction as judged from the ground temperature evolution at those sites (slow warming and cooling of the entire profiles) attributed to the existence of more fine-grained sediments. Mean monthly ground surface temperatures during the summer months barely exceed 6 °C at KCCo1. At KCCo2 only once – in July 2015 – the 6 °C-level was exceeded.

The general cool conditions at all three sites cause surface frost numbers (F+) indicating for all three sites permafrost conditions. For the coolest of the three sites, KCCo2, the mean F+ value indicates discontinuous permafrost (F+ = 0.62), whereas for the other two sites the two mean F+ values suggest sporadic permafrost (Table 3). However, in one warm year the F+ value at the rock glacier site in the HLC indicates even absence of permafrost. Table 3 lists furthermore the TDD for each sensor and each site. As shown, the number of TDD per year decrease

Table 3

Thermal conditions at the three ground temperature monitoring sites (HLCco, KCco1, and KCco2) between 2006 and 2015. HY = hydrological year; MAGST = mean annual ground surface temperature; MAGT = mean annual ground temperature (at different depths); F + = surface frost number (dimensionless); TDD = thawing degree days; SCD = snow cover days.

HLCco (2672 m asl; temperature sensors at 0, 30 and 100 cm depth)									
HY	MAGST (°C)	MAGT30 (°C)	MAGT100 (°C)	Gradient (C°/cm)	F +	TDD0 (°days)	TDD30 (°days)	TDD100 (°days)	SCD (days)
HY07/08	-1.43	-1.59	-2.08	-0.007	0.58	566	489	132	225
HY08/09	-0.37	-0.58	-1.28	-0.009	0.53	535	442	100	239
HY09/10	-1.29	-1.27	-1.65	-0.004	0.58	494	414	100	236
HY10/11	-0.72	-0.80	-1.76	-0.010	0.54	668	594	162	193
HY11/12	-0.72	-0.80	-1.78	-0.011	0.54	732	652	175	191
HY12/13	-0.29	-0.31	-0.90	-0.006	0.52	435	378	80	245
HY13/14	-0.70	-0.68	-1.03	-0.003	0.57	300	264	56	251
HY14/15	0.21	0.14	-0.82	-0.010	0.48	761	662	176	219
mean	-0.66	-0.74	-1.41	-0.008	0.54	561	487	123	225
KCco1 (2690 m asl; temperature sensors at 0, 10 and 50 cm depth)									
HY	MAGST	MAGT10	MAGT50	Gradient [C°/cm]	F + [0]	TDD0	TDD10	TDD50	SCD
HY06/07	-0.89	-1.05	-1.90	-0.020	0.54	712	557	58	29
HY07/08	-1.75	-1.64	-2.47	-0.015	0.59	612	493	22	112
HY08/09	-0.98	-1.15	-1.92	-0.019	0.56	513	399	9	224
HY09/10	-2.05	-2.16	-2.90	-0.017	0.60	560	475	5	88
HY10/11	-1.37	-1.50	-2.72	-0.027	0.56	715	643	2	41
HY11/12	-1.19	-1.34	-2.58	-0.028	0.56	740	647	0	86
HY12/13	-0.78	-1.04	-1.61	-0.016	0.56	437	381	0	206
HY13/14	-0.94	-1.09	-1.59	-0.013	0.58	405	358	4	176
HY14/15	Data gap								122
mean	-1.24	-1.37	-2.21	-0.019	0.57	587	494	13	120
KCco2 (2703 m asl; temperature sensors at 0, 10 and 20 cm [= ice surface] depth)									
HY	MAGST	MAGT10	MAGT20	Gradient [C°/cm]	F + [0]	TDD0	TDD10	TDD20	SCD
HY06/07	-1.66	-2.25	-2.61	-0.048	0.60	486	211	36	76
HY07/08	-2.08	-2.54	-2.96	-0.044	0.61	534	282	92	138
HY08/09	-1.49	-1.71	-1.87	-0.019	0.64	253	87	18	249
HY09/10	-1.76	-2.03	-2.22	-0.023	0.64	310	117	25	211
HY10/11	-1.69	-2.10	-2.39	-0.035	0.61	402	162	31	176
HY11/12	-1.34	-1.80	-2.04	-0.035	0.60	374	153	40	246
HY12/13	-1.10	-1.12	-1.38	-0.014	0.64	185	98	29	274
HY13/14	-1.03	-0.96	-1.13	-0.005	0.67	121	61	20	284
HY14/15	-0.20	-0.71	-0.99	-0.039	0.59	237	90	41	232
Mean	-1.37	-1.69	-1.96	-0.029	0.62	322	140	37	210

substantially from the ground surface inwards which has a strong influence on the potential heat transfer for permafrost and ice melt further into the ground. This decrease inwards is weakest at the coarse-grained rock glacier site HLCco where open voids are relevant for convective heat transfer causing similar TDD values at least at the uppermost two sensors. Therefore, Eq. (3) cannot be applied at this site. However, at the other two sites conductive heat transfer is important because the number of TDD at the lowest sensor approaches zero. Hence for those sites the sub-debris ice ablation has been estimated using the approach described in Eqs. (2) and (3). Results show that some 3.6 m of ice have been melted at site KCco1 yielding a mean annual rate of 0.361 m/a (Table 4) for the period 2006–2016. However, at site KCco1 the thickness of the supraglacial debris cover is not known exactly. A reasonable debris thickness of 1 m was estimated as judged from field evidences. At site KCco2 the calculated ablation during the 10 hydrological years was 9.4 m leading to an annual rate of 0.944 m/a. The thickness and variability of the debris layer plays an essential role in the spatial pattern of ablation rates in the KC but presumably also in the two rooting zones of the rock glacier in the HLC.

4.7. ERT results

The two ERT profiles in the HLC were substantially longer (490 and 290 m) compared to the 13 profiles in the KC (48 or 96 m) therefore the two HLC-profiles penetrate substantially deeper into the ground. The ERT profile H-1 reached a depth of c.100 m. The shorter and higher-elevated profile H-2 reached a penetration depth of c.55 m. Resistivity values of $\geq 100,000$ ohm·m have been interpreted by Kellerer-Pirklbauer et al. (2014) as a very conservative estimate for permafrost-influenced ground at the two ERT profiles in the HLC. Resistivity values at the lower profile H-1 reach maximum values of slightly more than

400,000 ohm·m. At this profile – and using the 100,000 ohm·m threshold – a maximum thickness of the permafrost body of about 20 m was revealed. In contrast, resistivity values at the higher elevated profile H-2 reach up to 1.6 Mio. ohm·m. At this profile a maximum thickness of the permafrost body of 30 m was revealed. In this permafrost body two distinct lenses (c.7–9 m thick) with resistivity values >1 Mio. ohm·m have been found under a 6–8 m thick superficial lower resistivity layer.

Fig. 10 depicts the results of the 13 ERT profiles measured in the KC. Results from the area around the LIA-moraine (K-1, K-2, K-3, K-4, and K-12) yield maximum resistivity values of between 51 k ohm·m (K-2) and 276 k ohm·m (K-12). Whereas the profiles K-1 to K-4 suggest the existence of only small lenses of frozen material and hence permafrost, the profile K-12 suggests substantially larger permafrost lenses with substantially higher resistivity values at the central part of the profile below a thin active layer. The two profiles K-5 and K-6 are located on SW-facing slopes at c.2735 m on the top of morainic sediments. Resistivity values at both profiles suggest permafrost lenses with a thickness of several meters below a thin active layer. However, a continuous permafrost lens does not seem to exist.

Profiles K-7 to K-9 have been measured near the estimated margin of the remaining debris-covered glacier remnant in the KC. Whereas some distinct small lenses of higher resistivity values suggesting permafrost have been found in the higher elevated profile K-7 (maximum value 105 k ohm·m), permafrost is most likely absent at the two profiles K-8 and K-9 with maximum resistivity values <10 k ohm·m. Results from the slightly lower elevated profile K-11 are comparable to the ones of profiles K-8 and K-9 although parts of the profile K-11 are drier and/or more coarse-grained hence yield higher superficial resistivity values. The remaining two profiles K-10 and K-13 (both crossing the glacier remnant) are substantially different to the other profiles with maximum values far above 10 Mio. ohm·m. In particular profile K-13

is of interest because it crosses the valley from south to north allowing the differentiation of a glacier remnant in the south (resistivity values <1 Mio. $\text{ohm}\cdot\text{m}$) from the marginally permafrost influenced terrain in north (sharp resistivity decrease with values <10 k $\text{ohm}\cdot\text{m}$).

5. Discussion

5.1. Surface and subsurface deglaciation and its impact on rock glacier formation

Glacier recession and the reduction of perennial snow existence in both studied cirques during the 166 year period c.1850–2016 deglaciated a 0.39 km^2 large area that is today subjected to subaerial weathering and geomorphic processes. Whereas the entire KC was glaciated during the LIA maximum, only the upper part of the HLC was covered by a glacier which overlaid the upper part of a larger rock glacier. Such overlapping situations have been also reported from other rock glaciers (e.g. Lugon et al., 2004; Ribolini et al., 2007, 2010). The glacier extent at HLC and KC of c.1850 was presumably also the maximum glacier extent during the entire Holocene (Lieb, 1987; Avian et al., 2005). Therefore, the LIA-glacier developed epigenetically on the top of the rock glacier which is at least 4000 years old (Avian et al., 2005). The weight of the LIA-glacier in the HLC increased the shear stresses applied onto the rock glacier potentially influencing the velocity and eventually pushing the rock glacier out of the cirque (Avian et al., 2005). The deglaciation in both cirques was relatively slow during the decades after the LIA maximum and very fast during the last two decades of the 20th century. This led to the almost absence of perennial snow in the HLC and to only small patches of surface ice and perennial snow in the KC. This is in general agreement to the observed deglaciation of the Austrian Alps (Fischer et al., 2015).

Despite the almost absence of subaerial ice in both studied cirques, ice exists below a debris layer in form of massive sedimentary ice or in form of congelation ice. Measurements of the debris cover thickness in the KC revealed a thin, several decimetre thick debris layer which covers large parts of the south-western part of the cirque. The supraglacial debris cover thickness increases downvalley. ERT measurements in the KC covering entirely (K-10) or partly (K-13) the debris-covered glacier remnant reveal a massive ice body with resistivity values exceeding 10 Mio. $\text{ohm}\cdot\text{m}$. Such values clearly point towards sedimentary ice (Kneisel and Hauck, 2008). Whereas the lateral boundary of the glacier ice was clearly identified in profile K-13, the subglacial topography was not reached in both profiles. This indicates a glacier remnant with a thickness of at least 20 m. Dark bands of ice have been observed at the

glacier remnant (Fig. 2E) indicating shear planes. Due to the valley-outward bending of the lower part of the tongue-shaped debris landforms (Fig. 7) which formed in the supraglacial sediments, it is argued that glacier movement at KC has not ceased so far.

Sub-debris ice ablation was calculated using ground temperature data from two sites in the KC and the one-dimensional heat-flux equation for conduction. Results revealed a total ice ablation of 3.6 m during the 10-year period 2006–2016 below a 1 m thick debris layer and, respectively, an ablation of 9.4 m below a 20 cm thick debris layer. At both sites the MAGST during the 2006–2016 period was negative and the calculated F_{+} -values point to permafrost conditions. However, in order to protect the remaining glacier mass in the KC from further melting, a debris cover thickness of few meters is necessary. The rate of debris production in the 200–300 m high cirque headwalls seems to be low (Kellerer-Pirklbauer and Rieckh, 2016) despite the heavily fractured rock (Krainer and Mostler, 2001). Therefore, the pace of debris production during the last decades was less than needed in order to protect the debris-covered glacier remnant in the KC from further melting. This further implies that the debris-covered glacier remnant in the KC has no potential to form a new glacier-derived rock glacier despite permafrost-friendly conditions as found out elsewhere (e.g. Monnier and Kinnard, 2015).

In the HLC massive sedimentary ice has been found at few places and only at the central and upper part of the rock glacier. The largest sedimentary ice exposure in the HLC has been made in the southern rooting zone of the rock glacier with an up to 20 m long and <2 m high ice outcrop at the southern side of a c.10 m deep spoon-shaped depression (i2 in Fig. 3C). This ice exposure is visually very similar to the one in the KC as depicted in Fig. 2E and therefore suggests accordingly a glacier remnant covered by a thin veneer of debris also at this site. The subsurface spatial extent of the sedimentary ice is not clear. However, as judged from substantial surface elevation lowering in the southern rooting zone as depicted in Fig. 8, the sedimentary ice does not only exist at the steep slope beneath the cirque headwall (as in the KC), but also extends into the rock glacier with low debris thickness values in the rooting zone. Similar massive sedimentary ice observations on both sides of a distinct – sometimes spoon-shaped and lake-filled – rooting zone depression have been made for other rock glaciers in the European Alps (e.g. Krainer and Mostler, 2000; Ribolini et al., 2007) or elsewhere (e.g. Kellerer-Pirklbauer et al., 2008).

The assumption of massive ice in the rock glacier is further supported by the horizontal displacement vectors in the southern rooting zone of the rock glacier as derived from aerial photographs from 1998 and 2002. As depicted in Fig. 5, the rock glacier part just north of the rooting zone depression is not moving outvalley as can be normally expected, but moves reverse back towards the cirque headwall related to higher ablation rates at the depression (thin debris layer) and lower ablation rates at the rock glacier itself (i.e. an effect of differential ablation) which led to a change in the surface geometry. Furthermore, the existence of ephemeral lakes in the rooting zone of a rock glacier has been observed at several other rock glaciers pointing to a massive ice-core (e.g. Krainer and Mostler, 2000; Ribolini et al., 2007; Kellerer-Pirklbauer et al., 2008).

Further indications for massive ice in the rock glacier of the HLC are the ERT results from the profile H-2 accomplished at the central part of the rock glacier (Kellerer-Pirklbauer et al., 2014). Two distinct lenses (c.7–9 m thick) with resistivity values >1 Mio. $\text{ohm}\cdot\text{m}$ have been detected suggesting the existence of massive sedimentary ice (Kneisel and Hauck, 2008). In contrast, no such high values have been found at the lower elevated H-1 profile with maximum values of only slightly more than 400,000 $\text{ohm}\cdot\text{m}$. According to Krainer and Mostler (2001) the morphology of the rock glacier in the HLC and the presence of a small shallow meltwater lake during the melt season in the southern rooting zone as well as the high surface flow velocity point to a glacial origin. Thus, these authors regard the rock glacier in the Hinteres Langtalkar to be an ice-cored or glacier-derived rock glacier which developed from a debris covered cirque glacier. This is in contrast to

Table 4

Calculated annual ice ablation beneath the supraglacial debris cover at sites KCco1 and KCco2. Parameters for site KCco1: debris thickness (h_d) = 1 m (estimated and taken as constant); thermal conductivity (k) = 0.22 $\text{W m}^{-1} \text{K}^{-1}$; measured temperature at the ground surface (T_s); estimated temperature of constantly 0 °C at 1 m depth (T_1) during summer; Parameters for site KCco2: debris thickness (h_d) = 0.2 m; thermal conductivity (k) = 0.22 $\text{W m}^{-1} \text{K}^{-1}$; measured temperatures at the ground surface (T_s) and at the debris-ice contact (T_i).

HY	Annual sub-debris ablation (m/a)	
	KCco1	KCco2
HY06/07	0.450	1.524
HY07/08	0.387	1.423
HY08/09	0.325	0.767
HY09/10	0.354	0.928
HY10/11	0.452	1.186
HY11/12	0.468	1.081
HY12/13	0.276	0.514
HY13/14	0.256	0.333
HY14/15	0.504	1.164
HY15/16 ^a	0.143	0.519
Sum 06/16	3.614	9.438
Mean 06/16	0.361	0.944

^a Data for the last 38 days of the hydrological year 2015/16 are missing.

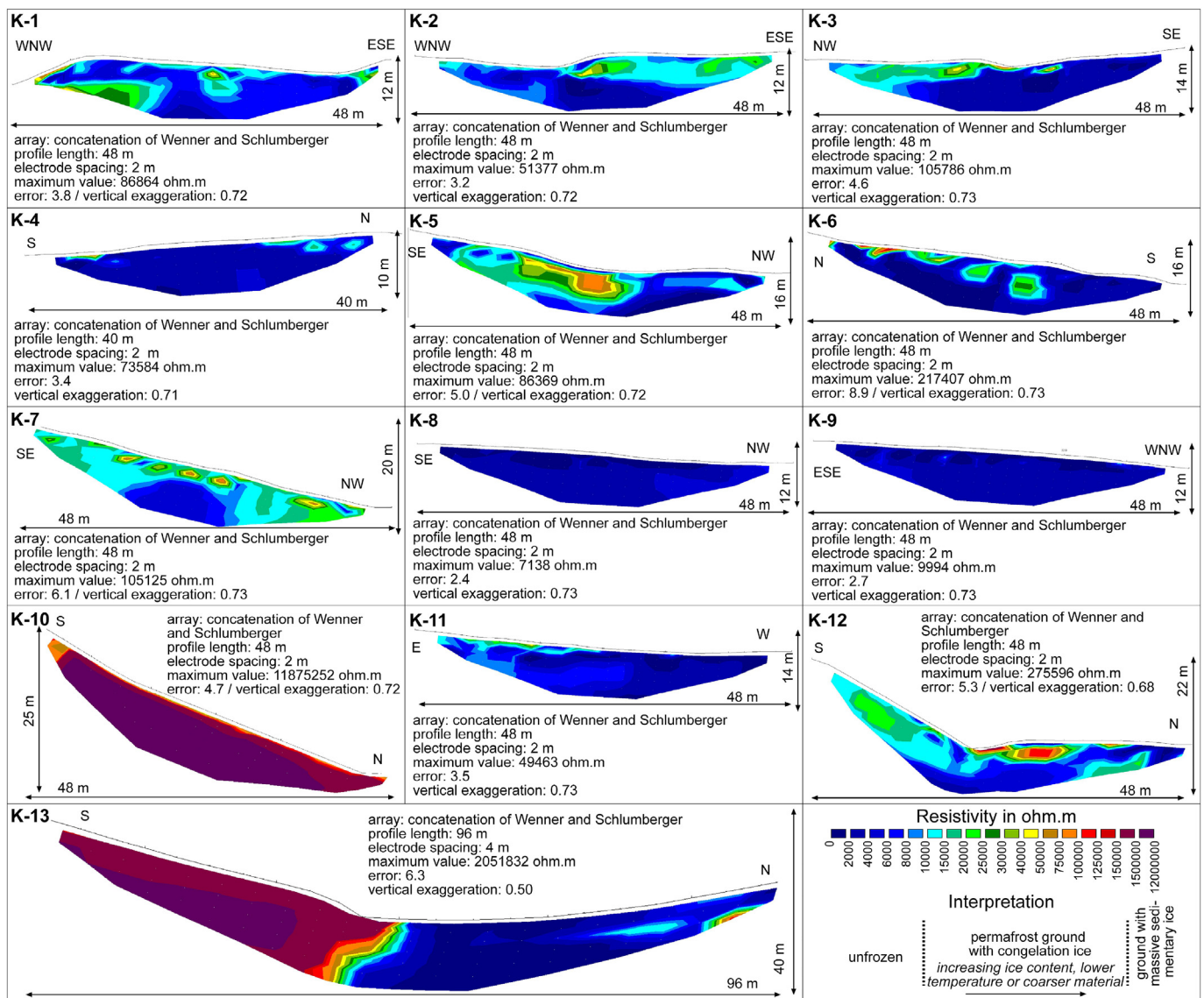


Fig. 10. ERT results in the KC based on concatenated Wenner and Schlumberger arrays. For location of profiles see Figs. 7 and 8. Interpretation according to the summaries in Kneisel (1999) and Kneisel and Hauck (2008).

other authors (Lieb, 1987; Avian et al., 2005) who considered this rock glacier as an ice-cemented or talus-derived rock glacier. No information about the internal structure of the rock glacier in the HLC was available for Lieb (1987), Krainer and Mostler (2001), and Avian et al. (2005). With the new results we can show that the upper and central parts of the rock glacier are surely to some extent ice-cored whereas the lower part is ice-cemented. This demonstrates that even single rock glaciers must be seen as glacial-periglacial transition landforms if time periods of several thousands years – normal for rock glacier formation and evolution (e.g. Krainer et al., 2015) – are considered. Such a rock glacier transition consideration has been as also reported by other studies in Europe (e.g. Ribolini et al., 2007, 2010) or elsewhere (e.g. Monnier and Kinnard, 2015; Janke et al., 2015).

5.2. Effects of deglaciation on geomorphology

In both cirques a number of small-scale, primarily tongue-shaped landforms were formed during the last decades in the glacier-underlain talus slopes below the cirque headwalls. An area of some 33,500 m² is covered by these 22 landforms in both cirques. The landforms are young geomorphic features formed during the last decades

presumably attributed to paraglacial slope adjustment processes (Kellerer-Pirklbauer and Kaufmann, 2007). The rock material at these landforms is different to the material found at adjacent slopes lacking such lobe structures. First, a diamict with both fines and coarse material must exist. Therefore, some sort of solifluction processes (Matsuoka, 2001) might be of relevance. Second, the coarse material fraction at such landforms in both cirques is in general smaller in size with more slabs and elongates compared to nearby non-deformed 'normal' scree slopes. All of the described tongue-shaped landforms seem to be very active according to their fresh geomorphic appearance with distinct fronts and the measured horizontal movement rates (Fig. 4C). However, the movement rate measured at the surface is the sum of the displacement of the supraglacial debris cover and the displacement of the remaining glacier ice mass due to glacier creep. The former is itself a combination of debris sliding at the surface of the glacier ice (impounding potentially at the footslope) and solifluction processes within the thin debris layer; cf. Matsuoka, 2001). Hence, the non-glacier part of the horizontal movement of the small-scale tongue-shaped landforms is less than measured at the surface and might be in the order of some tens of cm/a. Genetically, these lobes seem to be a mixture of an incipient rock glacier, a solifluction lobes and a landform which is related to a supraglacial debris

cover which slides downvalley at the interface between the debris layer and the underlying ice. A more genetic term for the observed lobes might be 'supraglacial solifluction lobes'.

The weight of the glacier which existed atop the rock glacier in the HLC most likely influenced the shear forces within the rock glacier. This force possibly caused higher surface velocities of the rock glacier despite cooler atmospheric conditions (causing in general lower surface velocity rates; Kellerer-Pirklbauer and Kaufmann, 2012) during that time (Fig. 3B). The mean annual surface velocities of the rock glacier in the HLC since the end of the 1960's showed relatively low values for both the upper and the lower part of the rock glacier (Fig. 4). This is in accordance to the cooler and glacier-friendly 1970s and early 1980s. A first peak in surface velocities was triggered by the warm summer of 2003 followed by a period of rock glacier deceleration. A second peak was reached during the last two years (2014/15 and 2015/16) with rates far higher than ever measured before (mean of 6 m/a for the lower part). The higher rates in the recent decades caused rock glacier disintegration (Avian et al., 2005, 2008, 2009) and continuous detachment of the main rock glacier body from its source (Kellerer-Pirklbauer and Rieckh, 2016). Basal sliding, as suggested also for similar rock glaciers (e.g. Krainer & Mostler, 2000), seems to be an important process to explain such high velocities at the rock glacier in the HLC. Such feasible basal sliding at the rock glacier in the HLC might take place at distinct shear zones within the permafrost body or between ice and debris (e.g. Arenson et al., 2002; Käab et al., 2006; Hausmann et al., 2007).

DEM differencing allowed the distinction of areas with mass gain and mass losses. Such a geodetically-based rock glacier mass balance analysis has the main limitation that changes in volume may have uncertain relationships with changes in mass (cf. Benn and Evans, 2010; p. 40–41). Furthermore, factors such as downslope movement of the rock glacier or a creeping talus slope, advection of local topographic features, compressive or extensive flow or melting or formation of ice within the landform further influence local changes of the surface elevation (e.g. Lambiel and Delaloye, 2004). For KC it was shown that in particular the area which is underlain by sedimentary ice experienced a substantial loss in volume with mean annual elevation changes of up to -86 cm/a. Further areas with significant surface elevation lowering are the LIA-terminal moraine and the north-eastern margin of the KC. At the former area several ERT profiles were measured indicating the existence of ground ice in very likely permafrost conditions. In particular profile K-12 suggests also ice-richer permafrost. The permafrost at this LIA moraine seems to be in a degrading state as suggested by field evidences with substantial ground subsidence (Fig. 2F). At the latter area with significant ground surface lowering permafrost was also detected by ERT profiles (K-5, K-6) with maximum values of >200 k ohm·m. The total change in volume in the studied part of the KC between 1998 and 2012 was $-249,926$ m³. Considering the LIA-moraine as a sediment trap (hence KC is a closed sediment transport system) one might conclude that at least some $17.850 (\pm 1300)$ m³ of ice (and to a smaller extent snow) have been melted each year on average in the KC during the period 1998–2012.

DEM differencing in the HLC covering the entire rock glacier reveals a more complex pattern during the 58-year period 1954–2012. Volume loss of the rock glacier in this period was 435.895 m³ indicating that this rock glacier is far from being in equilibrium supporting earlier observations (Kellerer-Pirklbauer and Rieckh, 2016). In none of the five considered periods (1954/74, 1974/98, 1998/02, 2002/06, 2006/12) a mean gain of mass has been observed. Whereas the mean annual surface elevation change was below average (-2.74 cm/a) during the first three periods, this rate was far above average during the last two periods indicating a substantially increase in mass loss since the beginning of this millennia. The pattern is in accordance to the deglaciation pattern shown in Fig. 3. This highlights the importance of considering decadal-scale geomorphic changes (cf. Micheletti et al., 2015) which is, however, strongly limited by the available remote sensing data but also by data quality such as shading effects or cloud coverage.

At the HLC, areas of substantial mass gain have been only observed at the rock glacier frontal part related to rock glacier advance. Areas of substantial mass loss are primarily located in the two rooting zones of the rock glacier and just above the rock glacier frontal part. Whereas the former is primarily related to massive sedimentary ice melting in the rooting zones, the latter is related to sedimentary ice melting, to permafrost thawing and to expansive dynamics and related rock glacier thinning causing rock surface lowering. Therefore, the surface elevation changes in the lower part of the rock glacier are a combination of the climatic and dynamical forcing.

5.3. The role of permafrost

Lugon et al. (2004) revealed in a study about permafrost and LIA glacier relationships in the Central Pyrenees, Spain, that a buried massive ice body could have been preserved on top of permafrost since the end of the LIA or earlier Holocene glacier advances. Morphological changes observed in their study caused by melting of buried glacier ice (see Fig. 8 in Lugon et al., 2004) formed structures similar to the one observed in the KC (Fig. 2F). These observations are in accordance that degrading glacier ice can survive for a long period of time below a protecting debris cover (Krüger and Kjær, 2000; Everest and Bradwell, 2003; Gómez et al., 2003) although the thickness of this protecting debris cover is essential as also shown by this study. The shielding effect is enhanced in permafrost areas with a shallow active layer, in particular where the thickness of the supraglacial debris-cover equals (or exceeds) the active layer thickness.

Discontinuous and sporadic permafrost exists at both studied cirques as revealed by ground temperature monitoring, ERT profiling, and regional permafrost modelling (Boeckli et al., 2012). However, the ERT profiles in the KC clearly show that permafrost is certainly not widely distributed even at elevations above 2700 m asl. The thickness of the active layer in both studied cirques is not known but as estimated from the ERT measurements it seems to be in the order of 1–3 m depending on slope aspect, substrate, elevation, and seasonal snow cover history. This implies that permafrost conserves only to some extent the buried sedimentary ice in both cirques particularly at the most-shaded sites. Meltwater is clearly audible at longitudinal depressions at the upper and central part of the rock glacier (Krainer and Mostler, 2001, 2002) suggesting a thin active layer and a impervious permafrost or sedimentary ice body. Such meltwater noises in the active layer are infrequent at the lower part of the rock glacier suggesting a less continuous permafrost body which is also influenced by rock glacier disintegration (Avian et al., 2008, 2009).

6. Conclusions

From the present study the following conclusions can be drawn:

- Our results indicate almost complete deglaciation of two cirques in alpine Austria since the end of the LIA. The deglaciation process was accompanied by debris-coverage of the receding ice mass leading to the formation and preservation of buried sedimentary ice. Such buried ice was confirmed by ERT measurements (identifying massive sedimentary ice), by differentiating of DEMs (distinguishing areas with substantial surface elevation subsidence), by quantification of horizontal displacement patterns of debris (backward movement), by hydrological observations (existence of an ephemeral lake) and by field observations.
- The ice-underlain slopes below the cirque headwalls formed in some areas of the two cirques distinct small-scale tongue-shaped landforms. Such landforms are restricted to diamicts. In contrast, coarser grained debris slopes show no sign of slope deformation. Horizontal velocity measurements at slopes with such lobes indicate rapid (order of 1 m/a) and relatively steady horizontal movement. The measured velocity is a mixed signal of the displacement of the supraglacial debris and the movement of the remaining glacier. The combined movement effect is mirrored by the bended shape of these landforms in the KC. It

is very unlikely that these lobes will form a new rock glacier in the KC because of the thin debris layer. In contrast, in the HLC the lobes nourish the existing rock glacier. The term 'supraglacial solifluction lobe' might be suitable for such landforms.

- DEM differencing has been applied at both cirques. The mean annual surface elevation change at the KC during the period 1998–2012 was 10.7 cm/a with maximum values of 86.0 cm/a yielding a total volume loss of $-249,926 \text{ m}^3$. This implies a mean annual ice (and snow) loss of $17.852 (\pm 1300) \text{ m}^3/\text{a}$. DEM data availability for HLC has been substantially better allowing to distinguish several different periods between 1954 and 2012. The mean annual surface elevation change was negative during all periods. Until 2002 the mean annual surface elevation change was in the order of 1.6 to 2.9 cm/a. This rate increased to 4.5 to 5.8 cm/a indicating a substantial increase in mass loss during the last 10 years with data.
- The combination of distinct mass losses as revealed by DEM differencing as well as the high rock glacier surface velocities during the last years increased the disequilibrium of sediment production in the rooting zone and sediment flux through the rock glacier. Therefore, the rock glacier is getting more and more in an 'unhealthy' state with no chance to recover.
- Ground thermal conditions and regional permafrost modelling indicate widespread permafrost existence. The seasonal snow coverage varied substantial from year to year and between the monitoring sites. Therefore, a significant trend of ground warming or cooling based on mean annual values of the period 2006–2016 was not detected for the ground monitoring sites used in this study.
- ERT profiles in both cirques helped essentially to understand ice distribution of the rock glacier in the HLC as well as the permafrost and glacier ice conditions in the KC. It was shown that the rock glacier in the HLC is both an ice-cored and an ice-cemented rock glacier depending on the area of interest. Ice melting of the rock glacier changed substantially the geomorphology and the surface flow pattern of this rock glacier in the recent past.
- ERT profiles in the KC allowed to identify a massive glacier remnant (>20 m) in the southern part of the cirque and the detection of smaller permafrost lenses in the higher parts of the cirque as well as at the complex LIA-moraines. Sedimentary and congelation ice from the LIA at these moraines is currently melting as indicated by field observations.
- The decadal-scale and multidisciplinary data presented in this study allow to give an in-depth view of the periglacial consequences of climate change and deglaciation in two adjacent alpine cirques. Many of the data used in this study are based on long-term observations hence highlight the need for long-term monitoring of permafrost and periglacial environments in order to gain deeper insights into the effects of climate change on high mountain environments.

Acknowledgments

This study was mainly funded by the projects ALPCHANGE, PermaNET, and permAfrost. 'ALPCHANGE – Climate Change and Impacts in Southern Austrian Alpine Regions' was financed by the Austrian Science Fund (FWF) through project no. FWF P18304-N10. 'PermaNET – Permafrost long-term monitoring network' was co-funded by the European Regional Development Fund (ERDF) in the scope of the Alpine Space Programme. Finally, 'permAfrost – Austrian Permafrost Research Initiative' was funded by the Austrian Academy of Sciences. Furthermore, the Hohe Tauern National Park authority of Carinthia provided several times logistical and financial support. Temperature data from the Observatory Hoher Sonnblick were kindly provided by Central Institute for Meteorology and Geodynamics (ZAMG), Vienna. In particular Alexander Doric, Michael Avian, Andreas Pilz, and Robert Stoffler are very much thanked for field work assistance. Two anonymous reviewers are very much thanked for their constructive criticisms and

valuable comments on an earlier version of this manuscript. The authors acknowledge the financial support by the University of Graz.

References

- Arenson, L., Hoelzle, M., Springman, S., 2002. Borehole deformation measurements and internal structure of some rock glaciers in Switzerland. *Permafrost. Periglacial Process.* 13:117–135. <https://doi.org/10.1002/ppp.414>.
- Avian, M., Kaufmann, V., Lieb, G.K., 2005. Recent and Holocene dynamics of a rock glacier system: the example of Langtalkar (Central Alps, Austria). *Nor. Geogr. Tidsskr.* 59, 149–156.
- Avian, M., Kellerer-Pirklbauer, A., Bauer, A., 2008. Remote sensing data for monitoring periglacial processes in permafrost areas: Terrestrial laser scanning at the rock glacier Hinteres Langtalkar, Austria. *Proceedings of the Ninth International Conference on Permafrost (NICOP)*, University of Alaska, Fairbanks, USA, June–July 2008, pp. 77–82.
- Avian, M., Kellerer-Pirklbauer, A., Bauer, A., 2009. LiDAR for monitoring mass movements in permafrost environments at the cirque Hinteres Langtal, Austria, between 2000 and 2008. *Nat. Hazards Earth Syst. Sci.* 9:1087–1094. <https://doi.org/10.5194/nhess-9-1087-2009>.
- Ballantyne, C.K., 1982. Aggregate clast form characteristics of deposits near the margins of four glaciers in the Jotunheimen Massif, Norway. *Norsk Geografisk Tidsskrift-Norwegian Journal of Geography* 36, 103–113.
- Ballantyne, C.K., 2002. Paraglacial geomorphology. *Quat. Sci. Rev.* 21 (18–19), 1935–2017.
- Barsch, D., 1996. *Rockglaciers. Indicators for the Present and Former Geocology in High Mountain Environments*. Springer, Berlin, p. 331.
- Benn, D.I., Ballantyne, C.K., 1993. The description and representation of clast shape. *Earth Surf. Process. Landf.* 18, 665–672.
- Benn, D.I., Evans, D.J.A., 2010. *Glaciers and Glaciation*. 2nd Edition. Hodder Arnold Publication, London, p. 802.
- Berthling, I., 2011. Beyond confusion: rock glaciers as cryo-conditioned landforms. *Geomorphology* 131, 98–106.
- Boeckli, L., Brenning, A., Gruber, S., Noetzi, J., 2012. Permafrost distribution in the European Alps: calculation and evaluation of an index map and summary statistics. *Cryosphere* 6:807–820. <https://doi.org/10.5194/tc-6-807-2012>.
- Brazier, V., Kirkbride, M.P., Owens, I.F., 1998. The relationship between climate and rock glacier distribution in the Ben Ohau Range, New Zealand. *Geogr. Ann.* 80A, 193–207.
- Delaloye, R., Perruchoud, E., Avian, M., Kaufmann, V., Bodin, X., Hausmann, H., Ikeda, A., Kääh, A., Kellerer-Pirklbauer, A., Krainer, K., Lambiel, C., Mihajlovic, D., Staub, B., Roer, I., Thibert, E., 2008. Recent interannual variations of rock glacier creep in the European Alps. In: Kane, D.L., Hinkel, K.M. (Eds.), *Proceedings of the Ninth International Conference on Permafrost (NICOP)*. University of Alaska, Fairbanks, USA, pp. 343–348.
- Deligne, P., 2005. Change in surface debris cover on Mont Blanc massif glaciers after the 'Little Ice Age' termination. *The Holocene* 15, 302–309.
- Etzelmüller, B., Hagen, J.O., 2005. Glacier-permafrost interaction in Arctic and Alpine Mountain environments with examples from southern Norway and Svalbard. In: Harris, C., Murton, J.B. (Eds.), *Cryospheric Systems: Glaciers and Permafrost. The Geological Society of London, London*, pp. 11–27.
- Everest, J., Bradwell, T., 2003. Buried glacier ice in southern Iceland and its wider significance. *Geomorphology* 52 (3), 347–358.
- Evin, M., Fabre, D., 1990. The distribution of permafrost in rock glaciers of the Southern Alps (France). *Geomorphology* 3, 57–71.
- Fischer, A., Seiser, B., Stocker Waldhuber, M., Mitterer, C., Abermann, J., 2015. Tracing glacier changes in Austria from the Little Ice Age to the present using a lidar-based high-resolution glacier inventory in Austria. *Cryosphere* 9:753–766. <https://doi.org/10.5194/tc-9-753-2015>.
- Gómez, A., Palacios, D., Luengo, E., Tanarro, L.M., Schulte, L., Ramos, M., 2003. Talus instability in a recent deglaciation area and its relationship to buried ice and snow cover evolution (Picacho del Veleta, Sierra Nevada, Spain). *Geogr. Ann.* 85A, 165–182.
- Graham, D.J., Midgley, N.G., 2000. Graphical representation of particle shape using triangular diagrams: an Excel spreadsheet method. *Earth Surf. Process. Landf.* 25, 1473–1477.
- Haeblerli, W., 1983. Permafrost-glacier relationships in the Swiss Alps – today and in the past. *Proceedings of the Fourth International Conference on Permafrost, Fairbanks, Alaska, USA, July 17–22, 1983*, pp. 415–420.
- Haeblerli, W., Hallet, B., Arenson, L., Elocin, R., Humlum, O., Kääh, A., Kaufmann, V., Ladanyi, B., Matsuoka, N., Springman, S., Vonder Muehl, D., 2006. Permafrost creep and rock glacier dynamics. *Permafrost. Periglacial Process.* 17:189–214. <https://doi.org/10.1002/ppp.561>.
- Hausmann, H., Krainer, K., Brückl, E., Mostler, W., 2007. Internal structure and ice content of Reichenkar Rock Glacier (Stubai Alps, Austria) assessed by geophysical investigations. *Permafrost. Periglacial Process.* 18:351–367. <https://doi.org/10.1002/ppp.601>.
- Humlum, O., 1998. The climatic significance of rock glaciers. *Permafrost. Periglacial Process.* 9, 375–395.
- Janke, R.J., Bellisario, A.C., Ferrando, F.A., 2015. Classification of debris-covered glaciers and rock glaciers in the Andes of central Chile. *Geomorphology* 241:98–121. <https://doi.org/10.1016/j.geomorph.2015.03.034>.
- Juen, M., Mayer, C., Lambrecht, A., Han, H., Liu, S., 2014. Impact of varying debris cover thickness on ablation: a case study for Koxkar Glacier in the Tien Shan. *Cryosphere* 8:377–386. <https://doi.org/10.5194/tc-8-377-2014>.
- Kääh, A., Frauenfelder, R., Roer, I., 2006. On the response of rock glacier creep to surface temperature increase. *Glob. Planet. Chang.* 56:172–187. <https://doi.org/10.1016/j.gloplacha.2006.07.005>.
- Kaufmann, V., Ladstädter, R., 2003. Quantitative analysis of rock glacier creep by means of digital photogrammetry using multi-temporal aerial photographs: two case studies

- in the Austrian Alps. Permafrost. Proceedings of the Eighth International Conference on Permafrost, 21–25 July. Vol. 1. A.A. Balkema Publishers, Zurich, Switzerland, pp. 525–530.
- Kaufmann, V., Ladstädter, R., 2010. Documentation and visualization of the morphodynamics of Hinteres Langtalar rock glacier (Hohe Tauern range, Austrian Alps) based on aerial photographs (1954–2006) and geodetic measurements (1999–2007). In: Kaufmann, V., Sulzer, W. (Eds.), *Grazer Schriften der Geographie und Raumforschung. Proceedings of the 10th International Symposium on High Mountain Remote Sensing Cartography (HMRSC-X)*, Kathmandu, Nepal, September 2008 Vol. 45, pp. 103–116.
- Kellerer-Pirklbauer, A., 2008. The supraglacial debris system at the Pasterze glacier, Austria: spatial distribution. Characteristics and Transport of Debris. *Zeitschrift für Geomorphologie*. 52 (Suppl. 1), 3–25.
- Kellerer-Pirklbauer, A., 2016. A regional signal of significant recent ground surface temperature warming in the periglacial environment of Central Austria. In: Günther, F., Morgenstern, A. (Eds.), *XI. International Conference On Permafrost – Book of Abstracts*, 20–24 June 2016. Bibliothek Wissenschaftspark Albert Einstein, Potsdam, Germany, pp. 1025–1026.
- Kellerer-Pirklbauer, A., Avian, M., Kaufmann, V., Niesner, E., Kuhnast, B., 2014. Climatic-induced spatio-temporal change of kinematics and ground temperature of rock glaciers and permafrost in the Hohe Tauern Range, Austria. In: Rutzinger, M., Heinrich, K., Borsdorf, A., Stötter, J. (Eds.), *permafrost – Austrian Permafrost Research Initiative. Final Report*, pp. 17–39.
- Kellerer-Pirklbauer, A., Bauer, A., Proske, H., 2005. Terrestrial laser scanning for glacier monitoring: glaciation changes of the Gößnitzkees glacier (Schober group, Austria) between 2000 and 2004. Proceedings of the 3rd Symposium of the Hohe Tauern National Park for Research in Protected Areas, Kaprun, Austria, September 2005, pp. 97–106.
- Kellerer-Pirklbauer, A., Kaufmann, V., 2007. Paraglacial talus instability in recently deglaciated cirques (Schober Group, Austria). Proceedings of the Ninth International Symposium High Mountain Remote Sensing Cartography (HMRSC-IX), Graz, Austria, September 14–22, 2006, pp. 121–130.
- Kellerer-Pirklbauer, A., Kaufmann, V., 2012. About the relationship between rock glacier velocity and climate parameters in central Austria. *Aust. J. Earth Sci.* 105 (2), 94–112.
- Kellerer-Pirklbauer, A., Lieb, G.K., Avian, M., Gspurning, J., 2008. The response of partially debris-covered valley glaciers to climate change: the example of the Pasterze Glacier (Austria) in the period 1964 to 2006. *Geogr. Ann.* (90 A):269–285 <https://doi.org/10.1111/j.1468-0459.2008.00345.x>.
- Kellerer-Pirklbauer, A., Lieb, G.K., Kleinfirchner, H., 2012. A new rock glacier inventory in the eastern European Alps. *Aust. J. Earth Sci.* 105 (2), 78–93.
- Kellerer-Pirklbauer, A., Rieckh, M., 2016. Monitoring nourishment processes in the rooting zone of an active rock glacier in an alpine environment. *Z. Geomorphol.* 60 (Suppl. 3):99–121. https://doi.org/10.1127/zfg_suppl/2016/00245.
- Kellerer-Pirklbauer, A., Wangenstein, B., Farbröt, H., Etzelmüller, B., 2008. Relative surface age-dating of rock glacier systems near Holar in Hjaltadalur, northern Iceland. *J. Quat. Sci.* 23, 137–151.
- Kneisel, C., 1999. Permafrost in Gletschervorfeldern. Eine vergleichende Untersuchung in den Ostschweizer Alpen und Nordschweden. *Trierer Geographische Studien* 22, 199 pp.
- Kneisel, C., 2003. Permafrost in recently deglaciated glacier forefields measurements and observations in the eastern Swiss Alps and northern Sweden. *Z. Geomorphol.* 47, 289–305.
- Kneisel, C., Hauck, C., 2008. Electrical methods. In: Hauck, C., Kneisel, C. (Eds.), *Applied Geophysics in Periglacial Environments*. Cambridge University Press, pp. 3–27.
- Krainer, K., Bressan, D., Dietre, B., Haas, J.N., Hajdas, I., Lang, K., Mair, V., Nickus, U., Reidl, D., Thies, H., Tonidandel, D., 2015. A 10,300-year-old permafrost core from the active rock glacier Lazaun, southern Ötztal Alps (South Tyrol, northern Italy). *Quat. Res.* 83: 324–335. <https://doi.org/10.1016/j.yqres.2014.12.005>.
- Krainer, K., Mostler, W., 2000. Reichenkar rock glacier: a glacier derived debris-ice system in the Western Stubai Alps, Austria. *Permaf. Periglac. Process.* 11, 267–275.
- Krainer, K., Mostler, W., 2001. Der aktive Blockgletscher im Hinteren Langtal Kar, Gößnitz Tal (Schobergruppe, Nationalpark Hohe Tauern). *Wissenschaftliche Mitteilungen Nationalpark Hohe Tauern* 6, 139–168.
- Krainer, K., Mostler, W., 2002. Hydrology of active rock glaciers: examples from the Austrian Alps. *Arct. Antarct. Alp. Res.* 34, 142–149.
- Krüger, J., Kjær, K.H., 2000. De-icing progression of ice-cored moraines in a humid, subpolar climate, Kötlujökull, Iceland. *The Holocene* 10, 737–747.
- Lambiel, C., Delaloye, R., 2004. Contribution of real-time kinematic GPS in the study of creeping mountain permafrost: examples from the Western Swiss Alps. *Permaf. Periglac. Process.* 15, 229–241.
- Lieb, G.K., 1987. Die Gletscher und Blockgletscher im Kärntner Teil der Schobergruppe. Unpubl. Doctoral thesis. Univ. Graz, p. 287 (in German).
- Loke, M.H., 2000. *Electrical Imaging Surveys for Environmental and Engineering Studies – A Practical Guide to 2-D and 3-D Surveys*. Penang, Malaysia. p. 67.
- Lugon, R., Delaloye, R., Serrano, E., Reynard, E., Lambiel, C., Gonzalez-Trueba, J.J., 2004. Permafrost and Little Ice Age glacier relationships, Posets Massif, Central Pyrenees, Spain. *Permaf. Periglac. Process.* 15, 207–220.
- Marangunic, C., 2010. Physical characteristics of rock glaciers in the mountains of central Chile. *International Glaciological Conference on Ice and Climate Change: A View from the South*, 1–3 February 2010, Valdivia, Chile.
- Matsuoka, N., 2001. Solifluction rates, processes and landforms: a global review. *Earth Sci. Rev.* 55, 107–134.
- Matsuoka, N., Ikeda, A., Date, T., 2005. Morphometric analysis of solifluction lobes and rock glaciers in the Swiss Alps. *Permaf. Periglac. Process.* 16, 1–17.
- Matsuoka, N., Murton, J., 2008. Frost weathering: recent advances and future directions. *Permaf. Periglac. Process.* 19:195–210. <https://doi.org/10.1002/ppp.620>.
- Mattson, L.E., Gardner, J.S., Young, G.J., 1993. Ablation on debris covered glaciers: an example from the Rakhiot glacier, Panjab, Himalaya. *IAHS Publ.* 218, 269–289.
- Mayewski, P.A., Rohling, E.E., Stager, J.C., Karlén, W., Maasch, K.A., Meeker, L.D., Meyerson, E.A., Gasse, F., van Kreveld, S., Holmgren, K., Lee-Thorpe, J., Rosqvist, G., Rack, F., Staubwasser, M., Schneider, R.R., Steigl, R.J., 2004. Holocene climate variability. *Quat. Res.* 62, 243–255.
- Micheletti, N., Lambiel, C., Lane, S.N., 2015. Investigating decadal-scale geomorphic dynamics in an alpine mountain setting. *J. Geophys. Res. Earth Surf.* 120:2155–2175. <https://doi.org/10.1002/2015JF003656>.
- Milk, T., 2016. Photogrammetrische Dokumentation der raumzeitlichen Veränderung von ausgewählten Blockgletschern in der Schobergruppe (Photogrammetric documentation of spatiotemporal changes of selected rock glaciers in the Schober Mountains, Austria). *Joannea Geol. Paläont.* 12, 45–52.
- Monnier, S., Kinnard, C., 2015. Reconsidering the glacier to rock glacier transformation problem: new insights from the central Andes of Chile. *Geomorphology* 238:47–55. <https://doi.org/10.1016/j.geomorph.2015.02.025>.
- Nelson, F.E., Outcalt, S.L., 1987. A computational method for prediction and regionalization of permafrost. *Arct. Alp. Res.* 19, 279–288.
- Nicholson, L., Benn, D.I., 2006. Calculating ice melt beneath a debris layer using meteorological data. *J. Glaciol.* 52, 463–470.
- Østrem, G., 1959. Ice melting under a thin layer of moraine and the existence of ice cores in moraine ridges. *Geogr. Ann.* 41A, 228–230.
- Reid, T.D., Brock, B.W., 2010. An energy-balance model for debris-covered glaciers including heat conduction through the debris layer. *J. Glaciol.* 56, 903–916.
- Ribolini, A., Chelli, A., Guglielmin, M., Pappalardo, M., 2007. Relationships between glacier and rock glacier in the Maritime Alps, Schiantala Valley, Italy. *Quat. Res.* 68:353–363. <https://doi.org/10.1016/j.yqres.2007.08.004>.
- Ribolini, A., Guglielmin, M., Fabre, D., Bodin, X., Marchisio, M., Sartini, S., Spagnolo, M., Schoeneich, P., 2010. The internal structure of rock glaciers and recently deglaciated slopes as revealed by geoelectrical tomography: insights on permafrost and recent glacial evolution in the Central and Western Alps (Italy–France). *Quat. Sci. Rev.* 29: 507–521. <https://doi.org/10.1016/j.quascirev.2009.10.008>.
- Ryder, J.M., 1971. The stratigraphy and morphology of paraglacial alluvial fans in south-central British Columbia. *Can. J. Earth Sci.* 8, 279–298.
- Sneed, E.D., Folk, R.L., 1958. Pebbles in the lower Colorado River, Texas, a study of particle morphogenesis. *J. Geol.* 66, 114–150.
- Staub, B., Hasler, A., Noetzli, J., Delaloye, R., 2016. Gap-filling algorithm for ground surface temperature data measured in permafrost and periglacial environments. *Permaf. Periglac. Process.* Published online. <https://doi.org/10.1002/ppp.1913>.
- Taucher, W., 2010. *Climatic Conditions of Six Selected Sites in the Hohe and Niedere Tauern Range 1961–2006*. Unpublished Master Thesis. University of Graz, p. 156.
- Taucher, W., Kellerer-Pirklbauer, A., Lieb, G.K., Avian, M., 2009. Climate change in Alpine areas in central Austria between 1961 and 2006. In: Bauch, K. (Ed.) *Proceedings of the 4th Symposium of the Hohe Tauern National Park for Research in Protected Areas, Kaprun, Austria, September 2009*, pp. 305–310.
- Wahrhaftig, C., Cox, A., 1959. Rock glaciers in the Alaska Range. *America*—>*Bull. Geol. Soc. Am.* 70, 383–436.
- Wegmann, M., Gudmundsson, G.H., Haeblerli, W., 1998. Permafrost changes in rock walls and the retreat of alpine glaciers: a thermal modelling approach. *Permaf. Periglac. Process.* 9, 23–33.
- Whalley, W.B., Martin, H.E., 1992. Rock glaciers: II models and mechanisms. *Prog. Phys. Geogr.* 16, 127–186.
- Wilson, P., 1990. Morphology, sedimentological characteristics and origin of a fossil rock glacier on Muckish Mountain, County Donegal, northwest Ireland. *Geogr. Ann.* 72A, 237–247.